Microwave Medical Imaging

Using Inverse Radon Transform and Quasi-Static Simulator

by

Saleh Ba Raean

A thesis

presented to the University of Waterloo

in fulfillment of the

thesis requirement for the degree of

Master of Applied Science

in

Electrical and Computer Engineering

Waterloo, Ontario, Canada, 2022

Author’s Declaration

I hereby declare that I am the sole author of this thesis. This is a true copy of the thesis, including any required final revisions, as accepted by my examiners.

I understand that my thesis may be made electronically available to the public.

Abstract

The features of Microwave Imaging (MI) drive its potential to be widely implemented in different fields. Its high penetration depth, comfortable usage, non-ionizing nature, and low-cost operation have attracted researchers in engineering and medical areas to use MI as an effective tool for medical imaging, remote sensing, and industrial imaging application (e.g., material fabrication and characterization). One of its most relevant and highly required application is to use it as an early-stage medical diagnostic tool for tumor detection as an alternative to conventional medical imaging approaches. MI can overcome the drawbacks of conventional medical imaging techniques like high operation frequency, high energy intensity, and relatively expensive operation (e.g., X-Rays and MRI). Therefore, in this work, we propose a novel technique for implementing MI as an effective imaging tool and implement that in the tumor detection and imaging process. In this study, numerical simulation in a Quasi-static environment is developed to model the imaging process of a body containing either one or more tumors. This model uses a movable and wavelength-independent electrostatic dipole point as a ray-like source to detect the hypothetically formed tumor. The variation of the power (electric field) of the waves generated from the vertically moving localized source that passes through a circular-like rotating object around its center is measured.

Accordingly, the projection profile for each point at an imaginary detection line (film) is registered. After that, Filtered Back Projection (FBP) and Inverse Radon Transform (IRT) algorithms are applied to reconstruct a 2D image of the scanned body. In order to reconstruct the body image, the power profile at different source elevations and different body angles are aggregated and processed using inverse Radon transform. Due to different dielectric properties (e.g., permittivity) of the object and the tumor, different measured power profiles are generated and therefore tumors can be detected. Simulations are performed for inhomogeneous and asymmetric structures. Results show the ability of the proposed method to numerically successfully reconstruct good-resolution images and the capability of distinguishing between abnormal and normal tissues.

The proposed method can be used as an early-stage and cheap approach for sensing abnormal bodies in human tissues as well as different upcoming applications.

Acknowledgments

First and foremost, I thank Allah, the Almighty, for helping me to successfully accomplish this work. Then, I want to express my deepest gratitude to my supervisor Prof. Omar M. Ramahi for his support, encouragement, and guidance. I am also grateful to my colleagues at the University of Waterloo, especially, Hamid Akbari Chelaresi, Seyed Hossein Mirjahanmardi, Rania Rabhi, Mohammed Alkatheri, and Maged Aldhaeebi for their support and collaboration.

Special thanks to all current and former Ramahi research group (ACR Laboratory) members, and all my friends at the University of Waterloo where I am so lucky to be part of this active and friendly environment. I am also thankful to the University of Waterloo for its valuable support and assistance.

I would like to express my most sincere appreciation towards Alsheikh Abdullah Bugshan for his unconditional support, guidance and endless generosity. Furthermore, I would like to express my acknowledge to the financial support of Hadhramout Foundation (HF) for their support during this difficult and unprecedented time.

Last but not least, I owe my endless gratitude to my dear parents (Mohammed Ba Raean and Fawzya Ba Gazie), my beloved wife (Sumyah Ba Raean), my brother (Abdullah Ba Raean), and all my family members for their patience, support, and unconditional love. Likewise, I want thank everyone who support and help me in completing this project.

Dedication

This is dedicated to my dear parents, my beloved wife (Sumyah), my daughter (Layan) and her future siblings, all my brothers and sisters, and all my beloved ones.

Table of Contents

List of Figures

List of Tables

List of Abbreviations

The Abbreviations used frequently in this thesis are provided in the table below.

CT	Computerized Tomography
CAT	Computerized Aided Tomography
MI	Microwave Imaging
NDT	Non-destructive Testing
MRI	Magnetic Resonance Imaging
USI	Ultrasound Imaging
PET	Positron Emission Tomography
ESA	Electrically Small Antenna
EM	Electromagnetic
RT	Radon Transform
IRT	Inverse Radon Transform
FST	Fourier Slice Theorem
DL	Deep Learning
FT	Fourier Transform
IFT	Inverse Fourier Transform
FFT	Fourier Fast Transform
BP	Back Projection
FBP	Filtered Back Projection
AR	Axial Ratio
2D	2-Dimensional
OUT	Object Under Test

Chapter 1
Introduction

1.1 Thesis Motivation

Creating a clear image of the interior details of a specific object plays a significant role in numerous areas, including material characterization[1], [2], manufacturing and industry applications, civil and environmental engineering, and medical imaging [2]. Nowadays, medical screening is done by various screening techniques such as Magnetic Resonance Imaging (MRI), X-Ray, and Ultrasound Scanning (USI). However, in the medical and Biomedical field, many researchers show potential interest in Microwave Imaging (MI) because it is a non-destructive testing (NDT) and due to its rapid imaging process and economical price[3]. Moreover, this modality can eliminate some of the conventional modality's disadvantages and limitations, such as high cost of operation, ionization, inconvenience for patients, low sensitivity and resolution, and harmful high-frequency radiation. The microwave detection and Imaging approach can introduce a reliable tool for medical imaging (e.g., mammography). Additionally, it can propose an alternative inexpensive, comfortable, non-ionizing (safe), and highly accessible detection and imaging technique for medical diagnosis and early detection, which can increase the survival opportunity of patients[4]. Since human body parts are non-magnetic and dielectric (naturally), and microwave region waves are able to penetrate inside dielectrics. Therefore, several microwave imaging systems were developed [2, 4, 6, 9] to meet the high demand for an alternative imaging technique.

Nevertheless, some problems including low resolution and simulation difficulty of the microwave imaging (MI) approach are not yet satisfactorily established, precisely in medical applications[5]. Thus, more developments in the field of image reconstruction and its algorithms are needed to prepare advanced microwave medical imaging technique.[6].

Breast cancer is considered as one of the main causes of death globally these days. According to the American Cancer Society, breast cancer is a disease which starts in the female breast (in one or both breasts) and the cells start growing out of control [1]. Furthermore, more than

40,000 females died because of breast cancer in the USA, in 2017 [7]. Correspondingly, about 250,000 new breast cancer cases were diagnosed in the US[7] , and maybe more than these numbers can be found around the world, specifically in the developing countries. For successful treatment, the detection in the early stages increases the opportunity for saving patients' lives. For several years, microwave radiometry has been applied for cancer detection and imaging in human bodies, which is considered as an adjuvant to mammography [4]. Many papers have introduced the usage of MI for detecting and imaging the tumors in women breasts by using low-frequency probes in the near-field region[8]–[11]. Near-field microwave sensors play a significant role in Microwave Imaging and Detection systems. Many previous projects have been done using traditional antennas such as monopole, patch, and printed dipole antennas as a transmitter and detector. As well, electrically-small probes (ESA) were also used to detect the tumors in the female breasts[12].

The detection principle of the microwave technique (MI) is based on the difference between healthy and malignant breast tissues using microwave Electromagnetic (EM) waves. According to some previous studies, abnormal breast cancer tumors exhibit sharp variation in their dielectric properties. Compared to normal tissues, malignant tumors have a higher value of the conductivity and permittivity parameters [2, 4, 12]. Electrically small antennas (ESA) have ray-behavior where they can penetrate the object under test (OUT) and record the change that occurs due to the change in the relative permittivity of the layers.

In this work, A localized and wavelength-independent (even in the very low-frequency range) source is used as an excitation source point for this image reconstruction approach because microwave imaging (MI) relies on the electrical properties contrast [4]. Furthermore, to overcome the drawbacks of simulation meshing and time, a quasi-static simulation environment is used to bring an accurate and rapid reconstruction process. The method of inverse Radon Transform [17] and Back-Projection (BP) are used for rebuilding the original image from its projection profiles.

1.2 Historical Overview and Previous Works

After the discovery of the X-ray, in 1895, Many works were developed in the field of imaging until James Radon (1917) published his reconstruction formula (Radon Transform). This formula has been used in solving several image reconstruction problems and developing the field of tomography[13]. In the period between 1940 and 1950, many technologies were discovered in this area, such as MRI, Ultrasound, and PEI. Furthermore, in 1972, the first CT medical scan was built by G. Hounsfield. After that, the technology of using X-rays and MRI have been used in the clinical stage. The first human MRI reconstructed image was taken in 1976[13]. Moreover, Positron Emission Tomography (PET) was discovered in 2000 by Townsend and Nutt. Regarding using microwave imaging (MI), Many scientific papers have studied this field to use this technology in the medical field. Therefore, in 2020, a new modality of using MI in the medical field as an imaging tool was discussed by S.H. Mirjahanmardi[2]. The near-field MI approach was introduced using low-frequency ranges and electrically-small probes for inhomogeneous and symmetric structures imaging. However, no imaging simulation was provided in this study. Consequently, this numerical simulation work is done to provide an imaging approach for asymmetric and non-homogenous structures.

1.3 Tomographic Image Reconstruction

Computerized Tomography (CT) is a non-invasive imaging technique[14] allowing for the visualization of the interior structures of an object without the superposition of over-lying and under-lying structures that usually affects conventional projection images[15]. For instance, in a conventional chest imaging, the ribs, heart, and lungs are all placed over each other's on one film (detection line), however a computed tomography (CT) slice takes each organ in its real 3D position. This tomography approach has been widely applied in several scientific areas, including physics, manufacturing, geophysical science, and treatment fields[16]. There are numerous modalities of tomography, such as ultrasound (USI), magnetic resonance (MRI), nuclear-medicine, and microwave imaging (MI) techniques[1]. The Radon transform and its inverse[17] provide the mathematical basis for reconstructing CT images from measured projections (scattering data), as will be discussed here.

1.4 Radon Transform and Filtered Back Projection (FBP)

The Radon transform (RT) is basically referred to the 2D projection profile obtained at each angle when we move the transmitter and receiver in parallel with each other and record the power (electric field intensity), for every single angle[18]. As shown in figure (1.1).

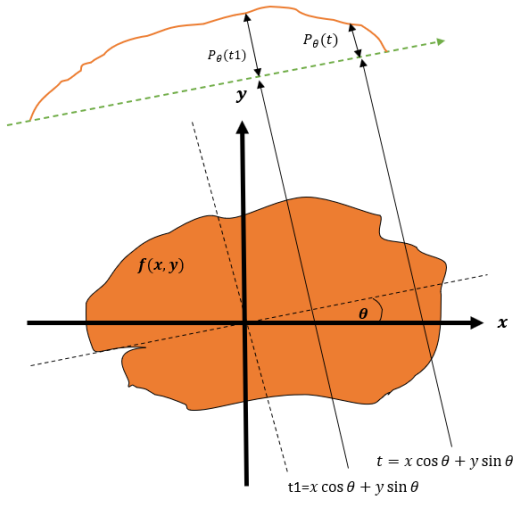

Figure 1.1: General planer of microwave imaging system

The most popular geometry of CT scanning is the parallel beams method[19]. In this method, the source (Tx) should move from the starting point to the ending point of the sweeping range. At the same time, the OUT should rotate (or by rotating the source beams) with a specific incremental. The geometry of the parallel-beams method is illustrated in figure (1.2).

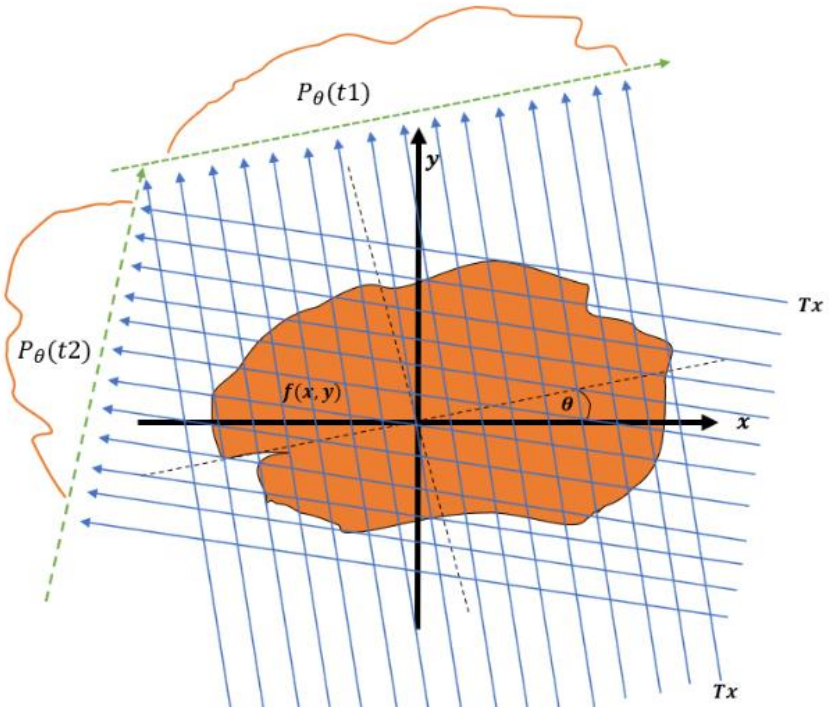

Figure 1.2: CT parallel beams method and its backprojection.

The movement and rotation of the point source through the object under test (OUT) will produce a power profile (P) at the detection line (film), where:

$$P_\theta(t) = \int_{(\theta,t)line} f(x,y)ds$$

And,

$$ds = \partial(xcos\theta + ysin\theta - t)dxdy$$

So, we can write that equation as,

$$P_\theta(t) = \int_{-\infty}^{\infty}\int_{-\infty}^{\infty} f(x,y)\ \partial(xcos\theta + ysin\theta - t)\ dxdy$$

The function $P_\theta(t)$ is defined as the Radon Transform of the function $f(x,y)$, and it is often referred to a (sinogram), because the Radon transform of an off-center point source is a sinusoid[14].

1.5 The Fourier Slice Theorem (FST)

The Fourier transform of each projection (Radon Transform, $g(\rho,\theta)$) is a slice of the 2-D Fourier transform (FT) of the original function $f(x,y)$, where this function describes the object under test (OUT).

$$\boldsymbol{F\big(f(x,y)\big) = F(u,v)} \;\&\quad \boldsymbol{F(g) = G(f)}$$

Figure (1.3) shows the transition from the Spatial domain (x,y) to the Frequency domain (u,v) using Fourier Transform (FT) along the angle (θ)[2] as well as its inverse.

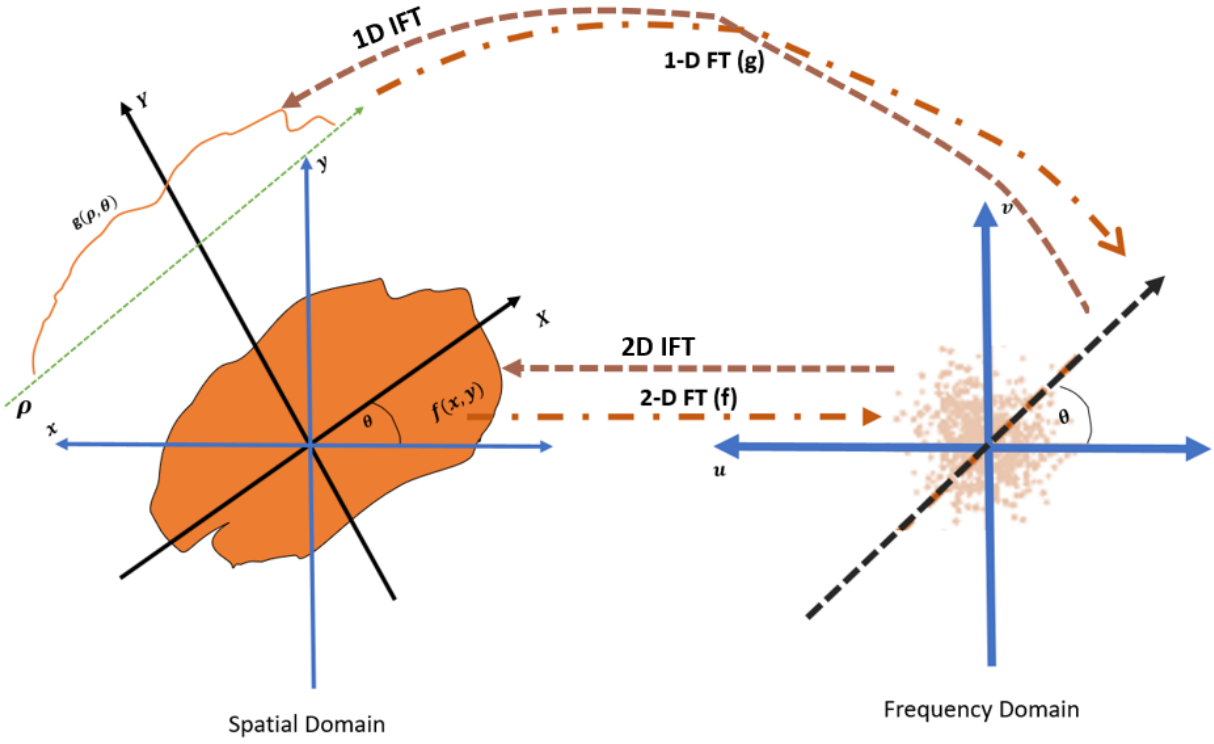

Figure 1.3: Fourier transform of $g(\rho,\theta)$ and $f(x,y)$ from the Spatial domain to Frequency domain along the (θ) angle and its inverse.

To prove the Fourier-slice theorem, we have the following equations:

$$G(f,\theta) = \int_{-\infty}^{\infty}\left[\int_{-\infty}^{\infty}\int_{-\infty}^{\infty} f(x,y)\delta(\mathrm{xcos}\,\theta + \mathrm{ysin}\,\theta - \rho)dxdy\right]e^{-j2\pi f\rho}d\rho$$

$$= \int_{-\infty}^{\infty}\int_{-\infty}^{\infty} f(x,y)\left[\int_{-\infty}^{\infty}\delta(\mathrm{xcos}\,\theta + \mathrm{ysin}\,\theta - \rho)e^{-j2\pi f\rho}d\rho\right]dxdy$$

$$= \int_{-\infty}^{\infty}\int_{-\infty}^{\infty} f(x,y)e^{-j2\pi f(\mathrm{xcos}\,\theta+\mathrm{ysin}\,\theta)}dxdy$$

$$= \int_{-\infty}^{\infty}\int_{-\infty}^{\infty} f(x,y)e^{-j2\pi(ux+vy)}dxdy\Big|_{u=\mathrm{fcos}\,\theta,v=\mathrm{fsin}\,\theta}$$

According to the transition from spatial to frequency domain, we know that,

$$u = f\cos\theta \quad \& \quad v = fsin\theta$$

$$G(f,\theta) = [F(u,v)]_{u=\mathrm{fcos}\,\theta,v=\mathrm{fsin}\,\theta}$$

Thus,

$$G(f,\theta) = F(\mathrm{fcos}\,\theta\,,\mathrm{fsin}\,\theta)$$

This equation describes the link between the original function, $f(x,y)$, and its projection (Radon Transform). where the FT of each projection $g(\rho,\theta)$ is equal to the FT of the OUT, $f(x,y)$, along the detection line (Film) with the same angle(θ).

1.6 Image Reconstruction

To reconstruct the original image,$f(x,y)$, a 2-D Inverse Fourier Transform (IFT) of the $G(f,\theta)$ should be taken to rebuild the original image, $f(x,y)$. As shown in figure (1.3).
Thus, the original image equation will be:

$$f(x,y)=\int_{-\infty}^{\infty}\int_{-\infty}^{\infty}F(u,v)e^{j2\pi(ux+vy)}dudv$$

And by using (the Jacobian transformation)[2], we will have:

$$dudv=\det\begin{vmatrix}\frac{\partial u}{\partial f} & \frac{\partial u}{\partial \theta}\\ \frac{\partial v}{\partial f} & \frac{\partial v}{\partial \theta}\end{vmatrix}dfd\theta$$
$$=f\quad dudv$$

Thus,

$$f(x,y)=\int_{0}^{2\pi}\int_{0}^{\infty}F(\mathrm{f}\cos\theta\,,\mathrm{f}\sin\theta)e^{j2\pi f(\mathrm{x}\cos\theta+\mathrm{y}\sin\theta)}fdfd\theta$$

$$f(x,y)=\int_{0}^{2\pi}\int_{0}^{\infty}G(f,\theta)e^{j2\pi f(\mathrm{x}\cos\theta+\mathrm{y}\sin\theta)}fdfdf$$

This can be simplified by using the Fourier transform (FT) features as following:

$$f(x,y)=\int_{0}^{\pi}\left[\int_{-\infty}^{\infty}|f|G(f,\theta)e^{j2\pi f\rho}df\right]_{\rho=\mathrm{x}\cos\theta+\mathrm{y}\sin\theta}$$

So, by solving those equation, we will have:

$$G(f,\theta) = \int_{-\infty}^{\infty} g(\rho,\theta) e^{-j2\pi f \rho} d\rho$$

This means that $G(f,\theta)$ is the Fourier transform (FT) of the Radon Transform, $g(\rho,\theta)$, with respect to ρ and θ as shown in figure (1.3).

1.7 Back Projection (BP)

The back-projection (BP) operation basically propagates the measured sinogram (Radon Transform, $g(\rho,\theta)$) back into the original object area along the projection paths from the detection line[20]. As illustrated in figure (1.4).

$$f_{Back-Projection}(x,y) = \int_0^{\pi} p(\rho,\theta)d\theta$$
$$= \int_0^{\pi} p\big((xcos\theta + ysin\theta),\theta\big)d\theta$$

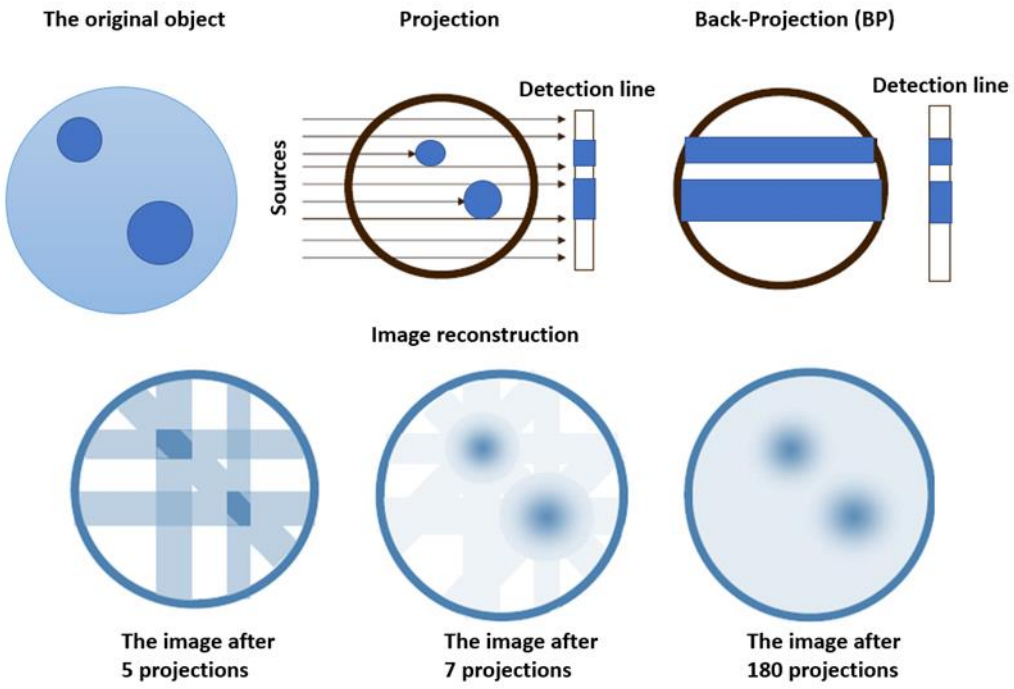

Figure 1.4: Backprojection process of the original image for different projections.

As we can notice, to make the reconstructed image sharp and clear, we should increase the projections number and eventually add all projection profiles together for reconstructing a sharp and clear image.

1.8 Filtered Back Projection (FBP)

The purpose of using filters is to increase the resolution of the reconstructed image. thus, sometimes we need to apply filters before reconstructing the desired image. Since the theorem

states that all projections need to be added to each other, the low-frequency parts will dominate the high-frequency, which contain detailed information, blocking the generation of a high-resolution image. Hence, we need to decrease the low-frequency parts. That is the reason that we need to multiply the projection profile by ramp-filter and hamming window (as we can use the IRadon function in MATLAB for this purpose). Ultimately, an IFT is required to be taken. Then all projection profiles should be added to each other to generate the image. Fortunately, MATLAB function (RADON) can do most of that.

In some cases, we need to apply filter processing (e.g., Padding, hamming window, Ramp filter, etc.) to make the reconstructed image sharper and non-blurry. Therefore, practically, Padding is required because of the periodic nature of Fourier transform (FT), especially in practical scanning due to the space limit. By Padding, we bring the periodic projection profile closer to what it is in practice[2].

For instance, in practice, if the scanning range is from -100mm to 100mm, then we should add padding for double the length of the scanning range from each side, making the projection profile looks from -500mm to 500mm. This is only done because the Fourier transform will be involved.

1.9 The Quasi-Static Simulator

Quasi-static solver has significant applications in electromagnetic (EM) modeling of transient phenomena. It is useful for a better understanding of the transition from statics to dynamics[21]. Moreover, it shows more interesting physics and more significant applications than statics because it provides a simpler way of solving the complex equations in 2D or 3D simulation with a noticeable decrease in the simulation time because it does not need large iterations number and complex matrix calculation process (complex mesh) [22]. The quasistatic models are also beneficial for a better understanding of both low-frequency electrodynamics and the transition from statics to electrodynamics[21]. Therefore, it is suitable for high resolution in dealing with lossy or dielectric materials. Usually, it uses for low-frequency bio-electromagnetic applications[23].

Starting from Maxwell's equations for E and B[24]. So:

$$\nabla . \mathrm{E} = \frac{\rho}{\varepsilon_0}$$

$$\nabla . \mathrm{B} = 0$$

$$\nabla \times \mathrm{E} = \frac{\partial B}{\partial t}$$

$$\nabla . \mathrm{B} = \mu_0 (J + \varepsilon_0 \frac{\partial E}{\partial t}).$$

Quasi-static simulation is obtained by neglecting $\frac{\partial B}{\partial t}$ in Fraday's law[23], therefore:

$$\nabla \times \mathrm{E} = 0$$

In the COMSOL simulation environment, obtaining the EM fields by considering stationary currents at every instant is possible (the quasi-static approximation). This approximation, as well, implies that the equation of continuity can be written as $\nabla \cdot \mathrm{J} = 0$. Also, the time derivative of the electric displacement (∂D/∂t) can be ignored in Maxwell-Ampère's law [25]. The quasi-static solver in COMSOL can eliminate the effects of wave propagation. Moreover, it can apply the charge relaxation theory of Ohm's law. Also, this approximation is valid to

provide that the variations in time are small and that the studied geometries are considerably smaller than the wavelength[25]. The AC/DC Module In COMSOL can offer a special environment of 2-D or 3-D electromagnetic simulation. It can operate quasi-static GUI with various types of physics, including Electrostatics, Magnetostatics, Electric currents, Electromagnetics, and EM in low-frequency simulations. In addition, this module is efficient for inhomogeneous and symmetric or asymmetric material simulation, and it can provide a quick and easy analysis[26].

Chapter 2
Simulation and Results

2.1 Source Design

Before starting the simulation, we want to identify the suitable source for the quasi-static simulation environment. Therefore, two charges (small dipole) with the same size and a specific separation distance (d) are used in different directions (x,y, and z). These two charges are contrasting in charge signs (-q and +q)[24].

In COMSOL, the Electrostatic Point Dipole source was used because it symbolizes the limiting circumstance of zero separation distance (infinitesimal separation) between two equal source points of opposite charge signs (q). At the same time, keeping the product between separation distance (d) and source strength at a fixed value which called the dipole moment direction[24].

$$p = qd$$

The dipole moment is a vector entity with the positive direction from the negative charge (q-) to the positive charge (q+). As it is shown in figure (2.1).

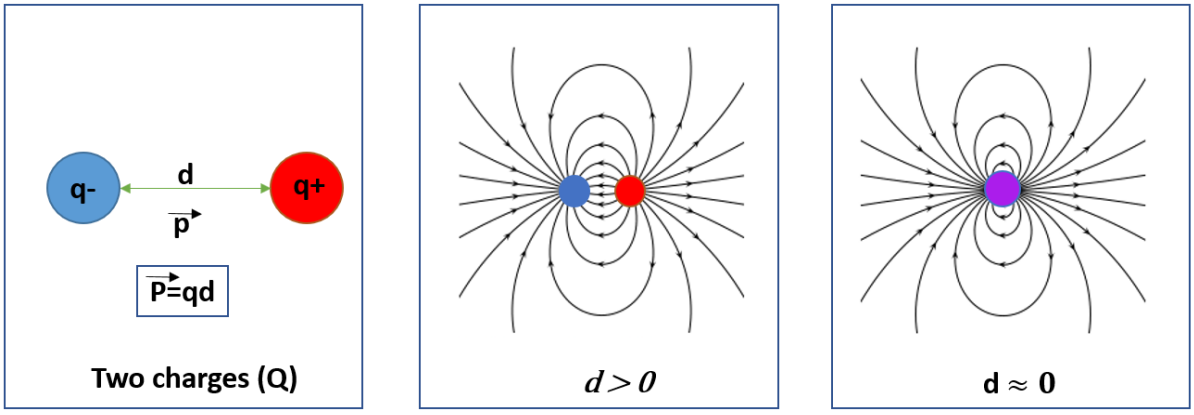

Figure 2.1: The electric fields of two charges with different distances.

2.2 Source Polarization

To find the suitable source for this approach, different polarized sources were tested for the best sensitivity to the dielectric properties changes.

2.2.1 Y-Polarized Dipole Source

Two charges in the Y-axis direction are considered as a source for this simulation section. This source is positioned at a distance (d) from the OUT. Figure (2.2) and table (1) show the geometry and the parameters for this simulation.

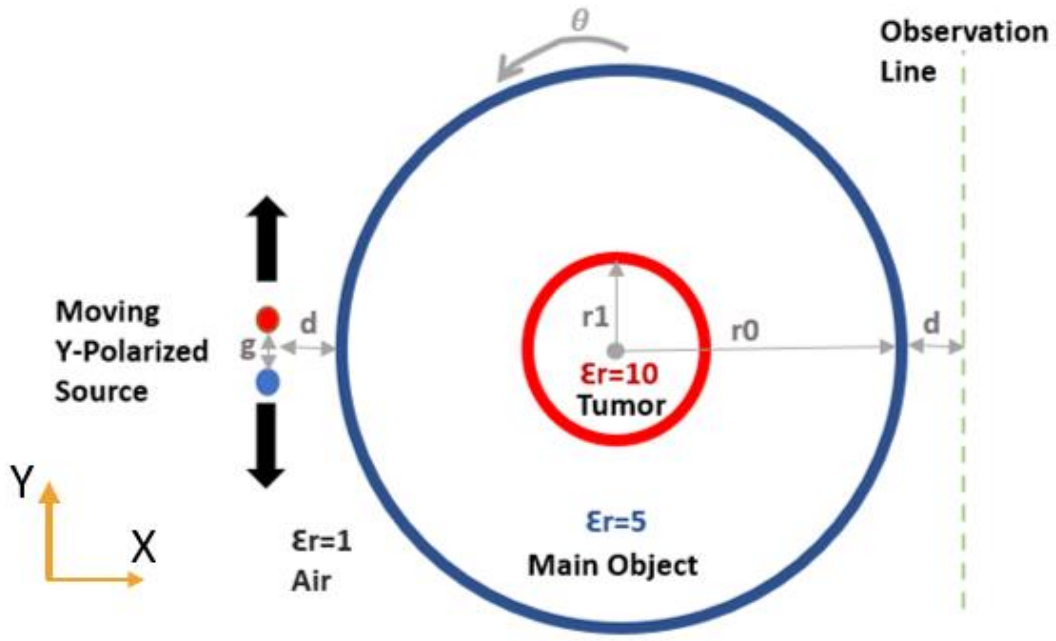

Figure 2.2: The geometry of one tumor and a source in Y-Direction.

The AC/DC module in COMSOL is used to simulate this design where the design was built using the parameters that defined in table (1).

Table 1. Image Reconstruction Design Parameters

Parameter	Value
d	2 mm
r0	25 mm
r1	5 mm
θ	0:5:180 degree.
y0	-35:1:35 mm
g	1 mm

From COMSOL, the electric field profiles (E^2) for each source position (y0) according to the object (OUT) rotation (0-180 degree) is measured as shown in figure (2.3).

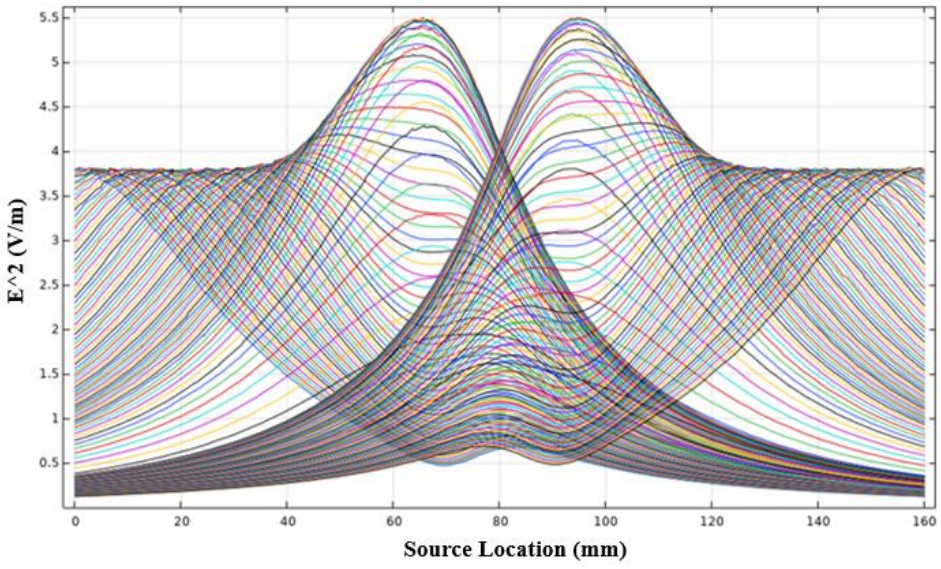

Figure 2.3: The electric fields profile (E^2) for each source position (y0) according to the rotation angles in Y-direction.

To display the Radon Transform (RT) projection function (g) for each position, MATLAB software tool [30] was used to perform this function as illustrated in figure (2.4).

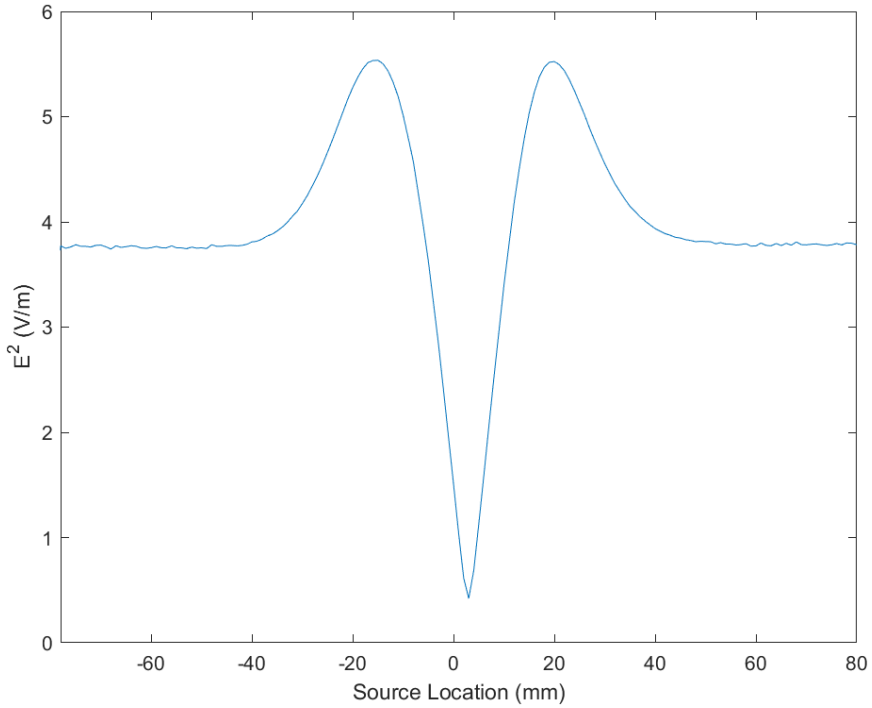

Figure 2.4: The electric filed as a function of a source location (Y-Polarized).

In addition, to examine the sensitivity of this source, different geometries of inserted bodies (Tumors) in different sizes, positions, and relative primitivities were simulated, as figure (2.5) indicates.

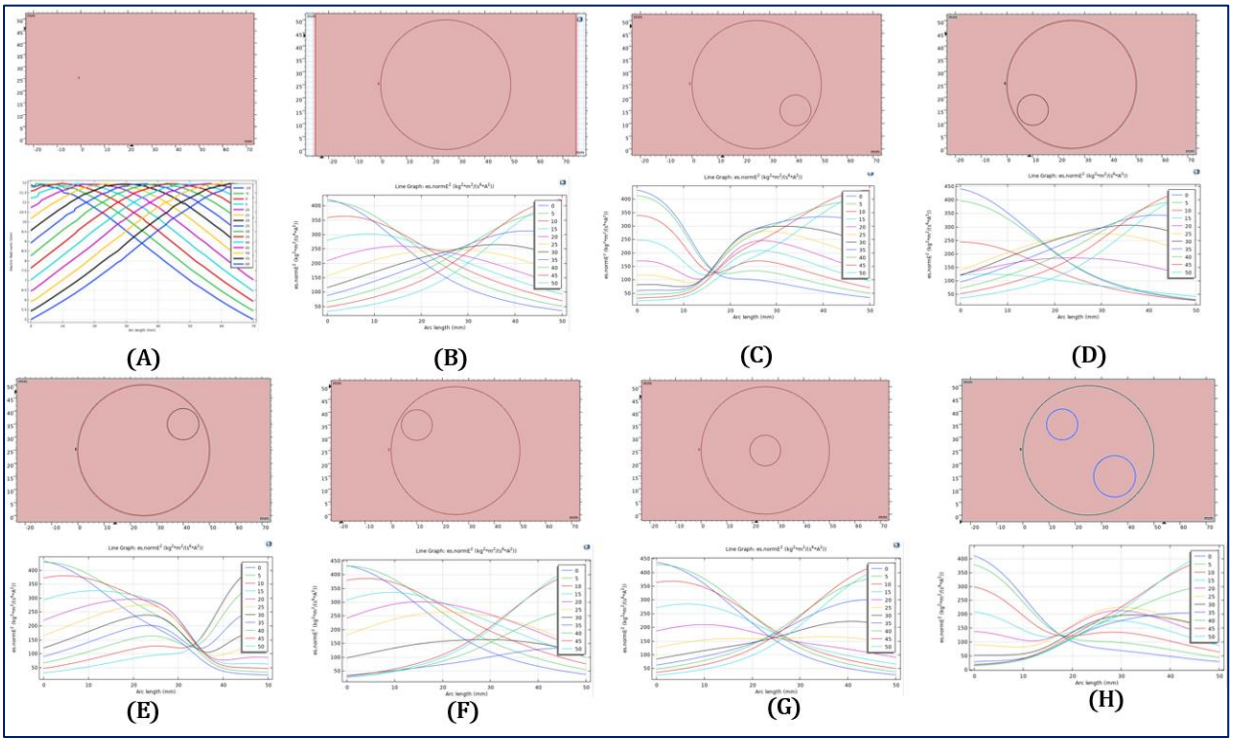

Figure 2.5 The electric field (radiated power) profiles as a function of source location for different geometries: A. a source in the air. B. a source and a main circle with $\varepsilon_r = 5$. After adding a tumor with $\varepsilon_r = 20$, radius (r0) $= 10$, located at (x,y): C.(35,15), D.(10,15), E.(35,30), F.(10,35), G.(0,0). H. Two tumors with $\varepsilon_r = 10\ \&20$, r0 $= 20\ \&10$ and placed at (30,10) and (10,30), respectively.

2.2.2 Z-Polarized Source

The same steps of simulation were repeated as in the previous section. However, the source became a point source (Line charge). The moment direction (p) is out of the plane (in Z-direction) as illustrate in figure (2.6).

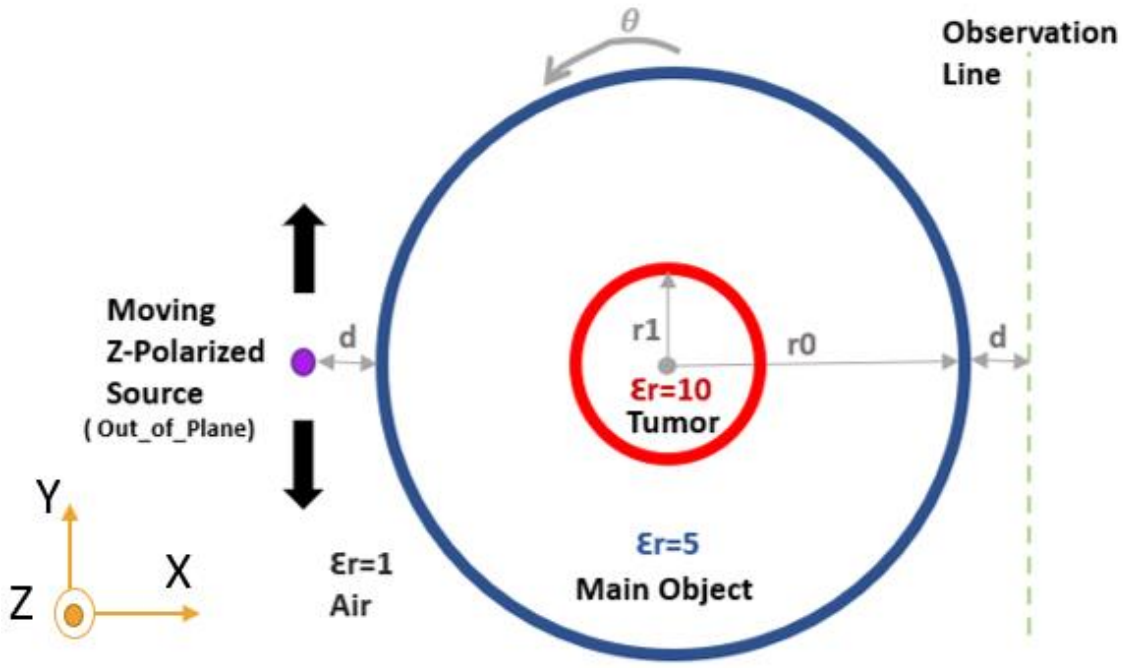

Figure 2.6: The geometry of a tumor and a source in Z-Direction.

The electric field profiles and Radon Projection of this case are shown in figures (2.7 and 2.8). According to the results, there is a noise in the projection profile peak. As a result, this noise will decrease the sensitivity of this source and the ability to detect any change in the dielectric properties. Thus, we cannot use this source in this work.

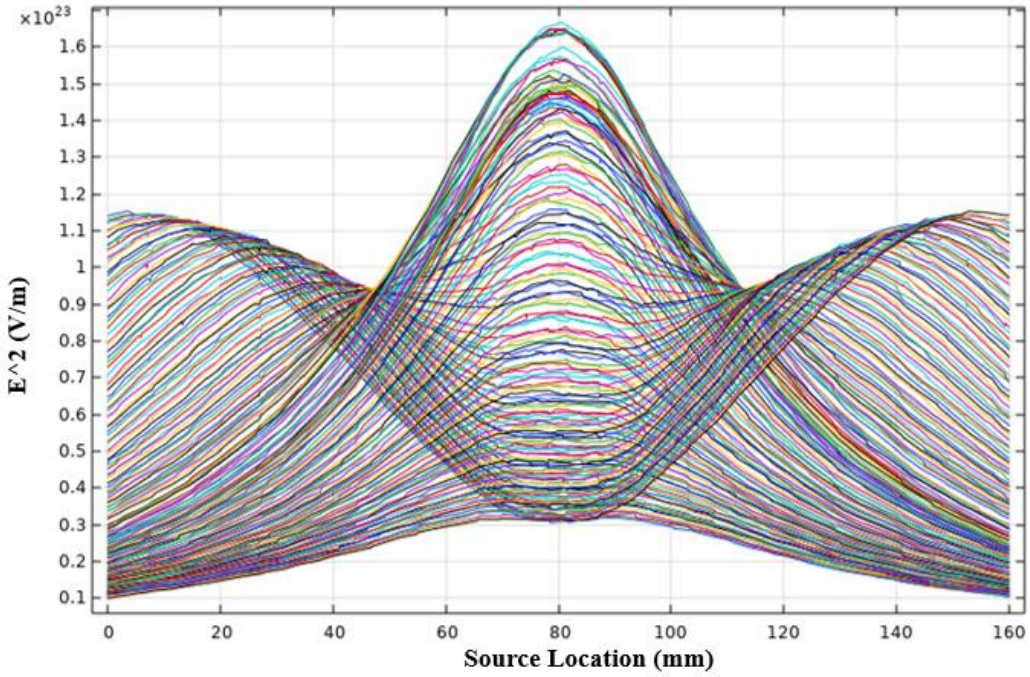

Figure 2.7: The electric fields profile (E^2) for each source position (y0) according to the object rotation angles in Z-direction.

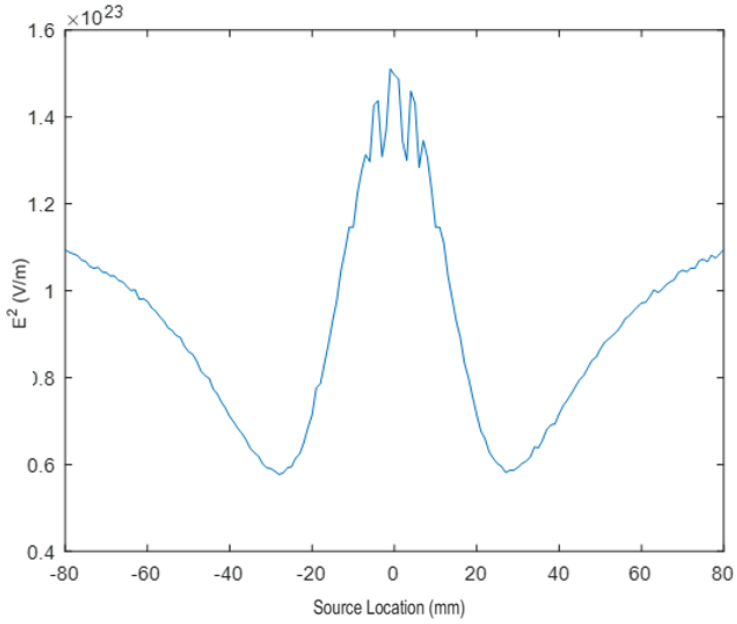

Figure 2.8: The electric filed profile as a function of a source location (Z-Polarization).

2.2.3 X-Polarized Source

When two charges are located horizontally (in the X-axis direction), they will act as a dipole point source as what we did in this simulation. Figure (2.9) shows the X-polarized source consists of two charges, and the gap (g) between them is extremely small.

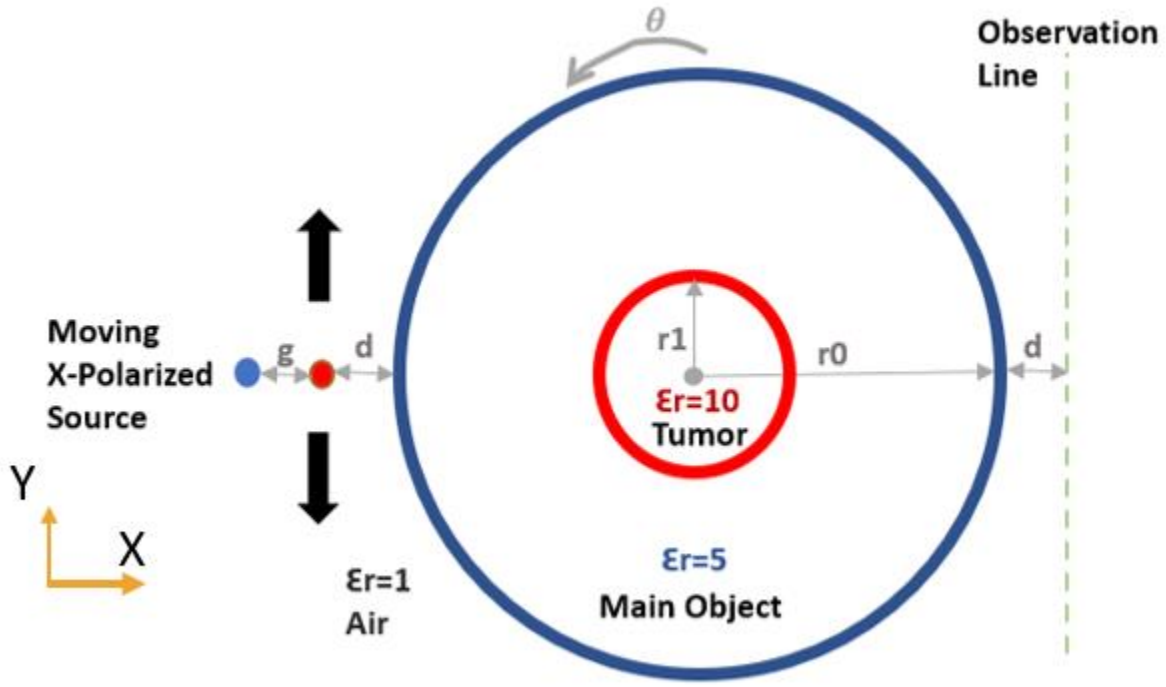

Figure 2.9: The geometry of a tumor and a source in X-Direction.

Furthermore, the electric field profiles, as well as the Radon Projection of this case, are shown in figures (2.10 and 2.11). According to these figures, there is no noise in the projection profile in this case. Therefore, the sensitivity of this source is high, and it can detect the changes easily.

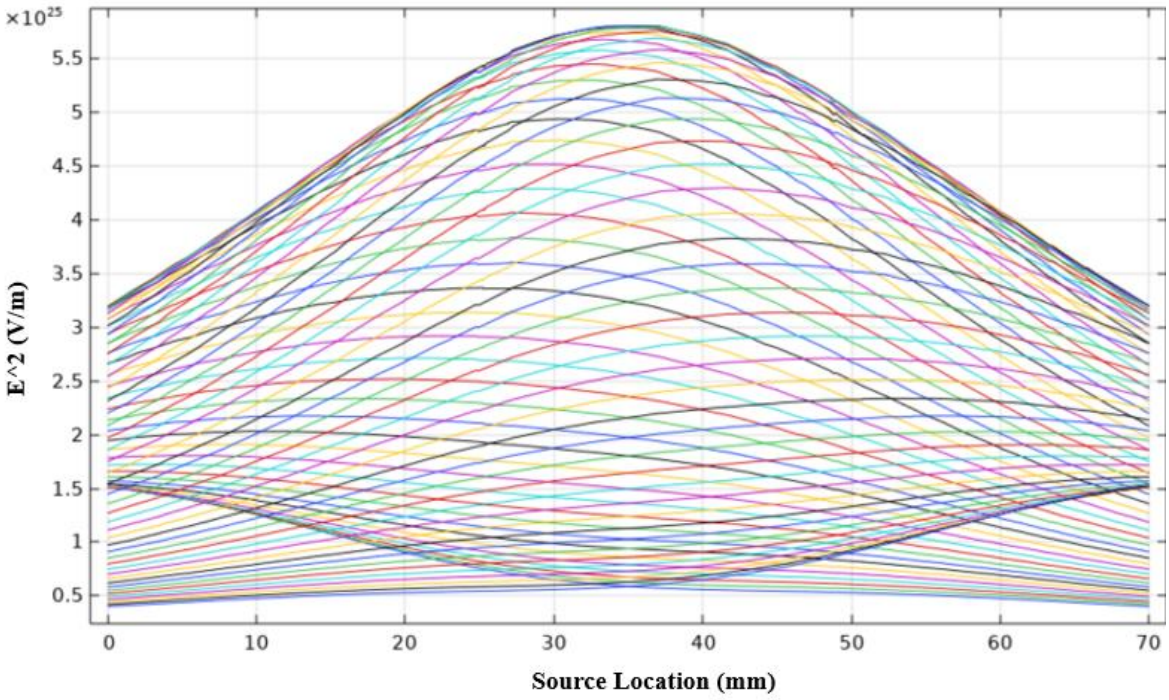

Figure 2.10: The electric fields profile (E^2) for each source position (y0) according to the object rotation angles in X-direction.

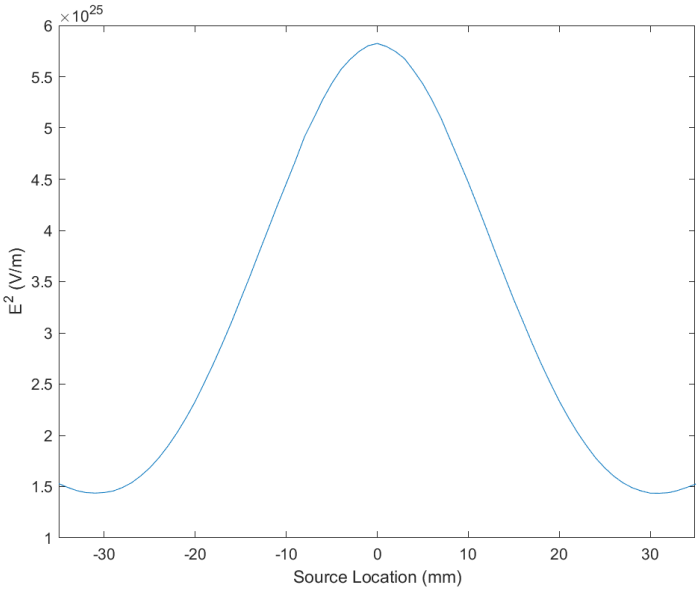

Figure 2.11: The electric filed as a function of source location (X-Polarized).

We can notice that X-Polarization is the best one among the three types because of its high sensitivity in detecting the changes in the medium dielectric properties. In COMSOL, we can use a point to represent two opposite charges with an infinitesimal separation. This source is called the electrostatic dipole point source and its moment direction is the X-axis direction. The electric field projection profile is shown in figure (2.12).

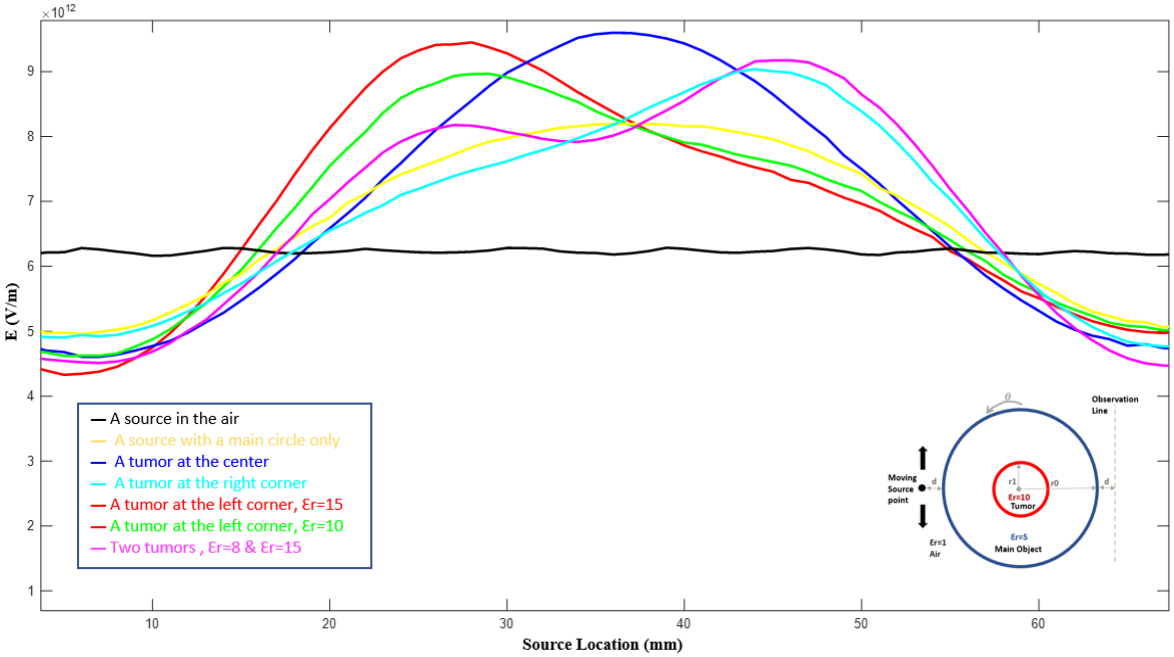

Figure 2.12: The electric filed profile as a function of source location for different geometries.

2.3 Image Reconstruction Simulation

In this section, Microwave Imaging will be conducted to image an abnormal inserted body (tumor) inside a normal tissue. This simulation is for inhomogeneous materials, and the distinguishing between the healthy and the tumorous body is done by differentiating the relative permittivity for each. We have studied several cases of imaging in this work as following.

2.3.1 Symmetric circle case

In this case, the unhealthy body is inserted in the center of the main body, as illustrated in figure (2.13).

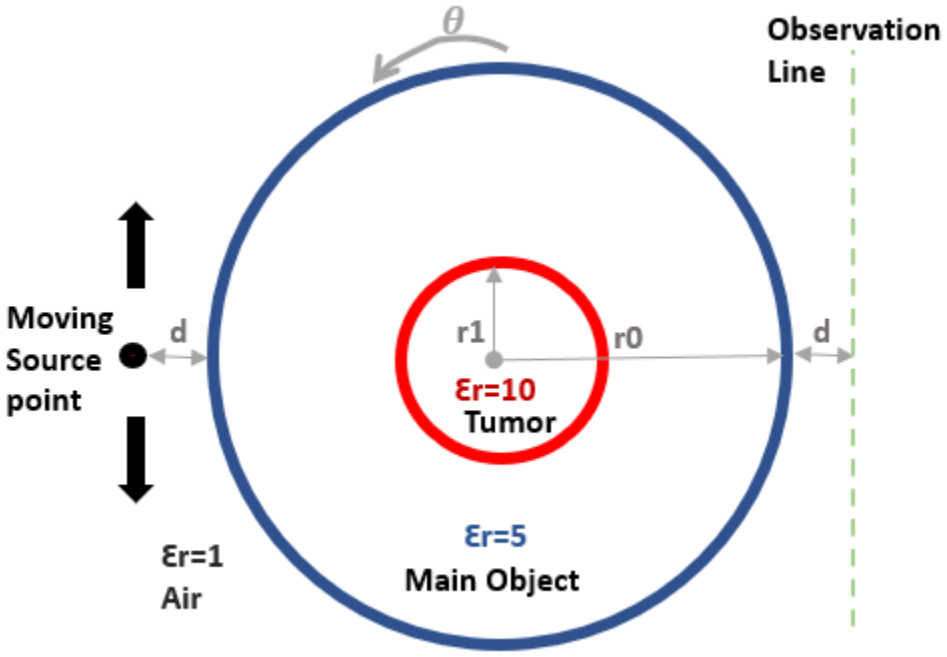

Figure 2.13: The geometry of one tumor in the center of the main body.

COMSOL is used to simulate this case, while MATLAB (IRADON Function) is used to find the Sinogram (Radon Transform), as indicated in figure (2.14). Moreover, figure (2.15) shows the reconstructed image for the symmetric case.

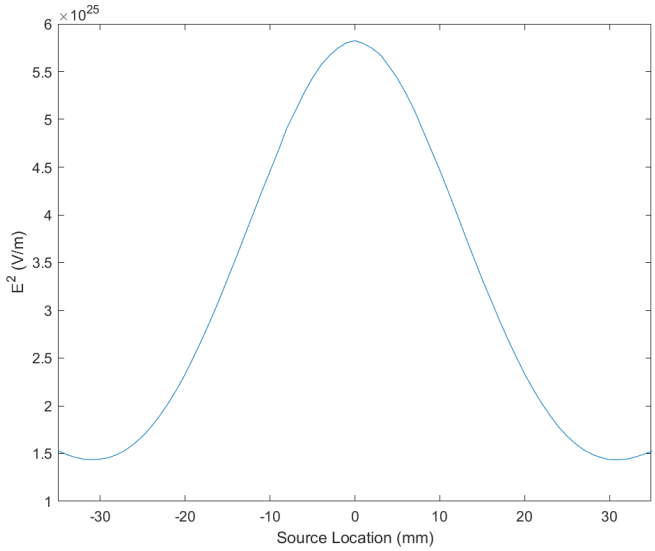

Figure 2.14: The electric filed projection as a function of source location.

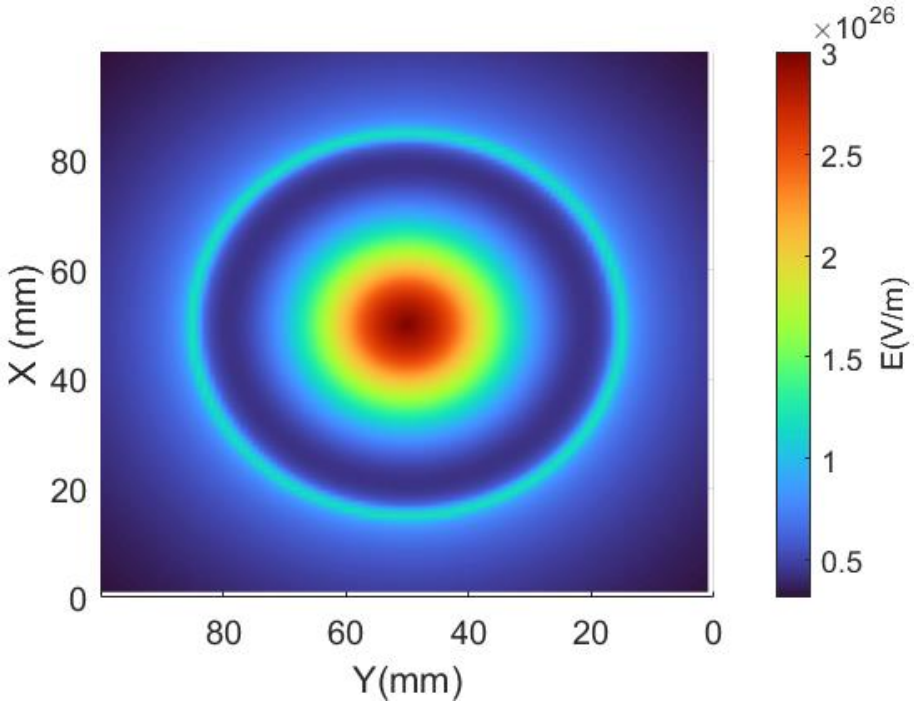

Figure 2.15: The reconstructed image in the symmetric case.

2.3.2 Symmetric ring case

In this section, the central circle was replaced by a ring with a width of (w=2mm). The relative permittivity of this ring is higher than the permittivity of the main circle and the inner circle. Figure (2.16) illustrates the geometry of this case.

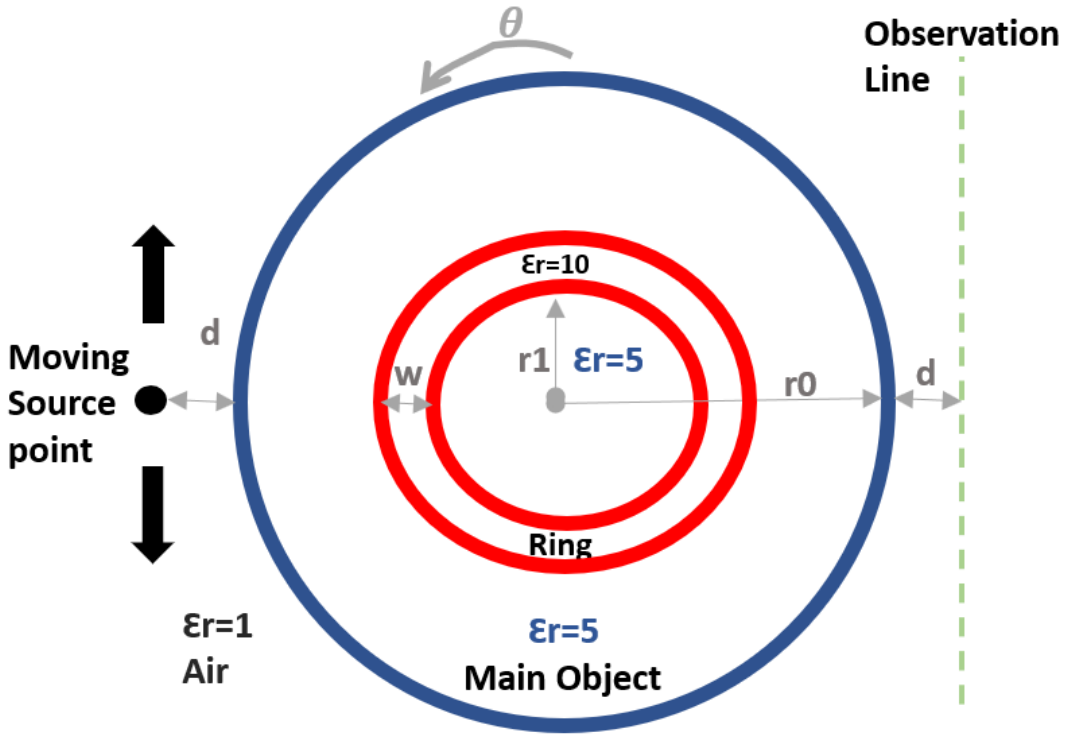

Figure 2.16: The geometry of a ring in the center of the main object.

By following the same process, the sinogram and the reconstructed image of the ring are shown in figure (2.17) and (2.18), respectively.

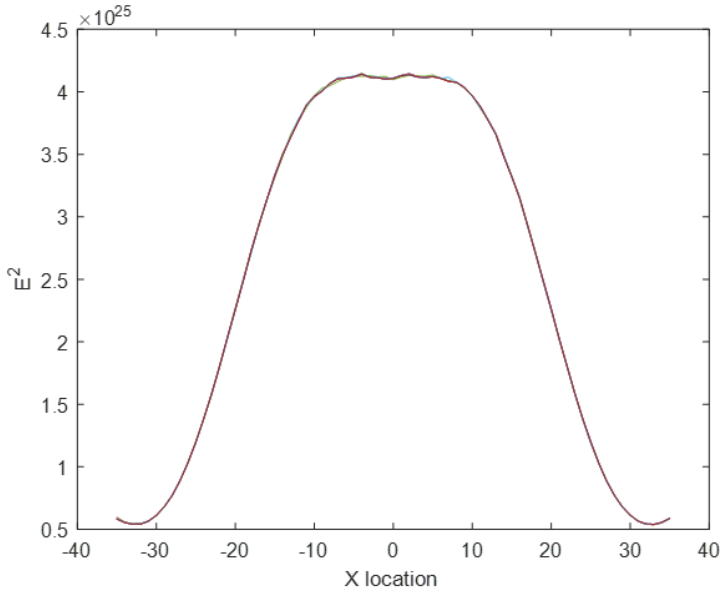

Figure 2.17: The electric filed projection profile as a function of source location.

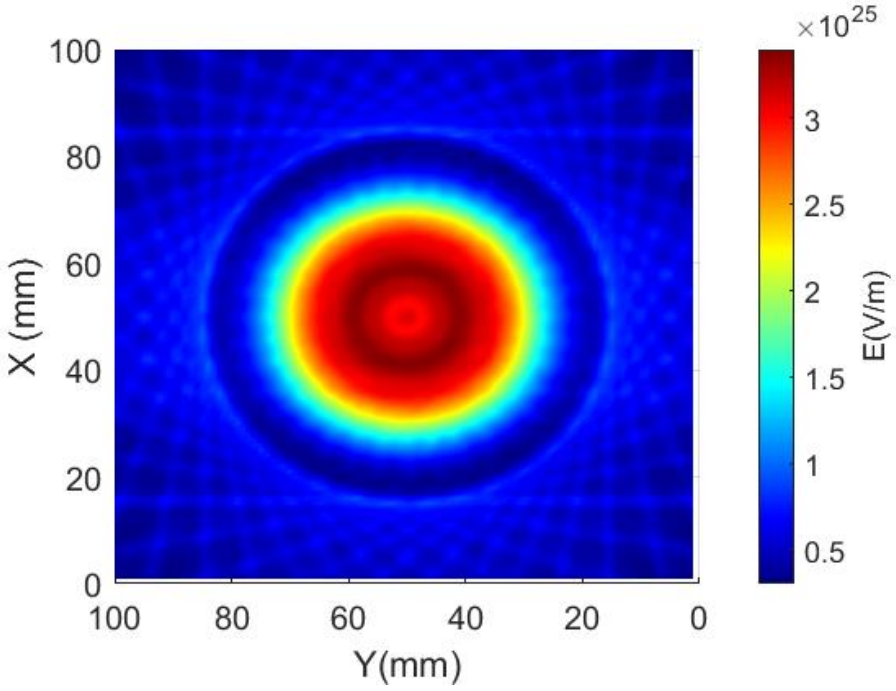

Figure 2.18: The reconstructed image of the ring in the symmetric case.

2.4 Asymmetric cases

Reconstructing an inhomogeneous and non-symmetric image is harder than rebuilding a symmetric image because the reconstruction process needs more steps (moving and rotating), and this will take more time. In this work, we have used a 2D Quasi-static simulator to minimize the simulation time and decreasing the meshing process because quasi-static simulator does not require huge iterations and calculations. Some asymmetric cases are considered in the following sections.

2.4.1 One Asymmetric Tumor

In this part, an inserted body was located at the position (x,y)= (10,20)mm (the upper left corner). This geometry of this case is shown in figure (2.19) while the design parameters are indicated in table (2.1).

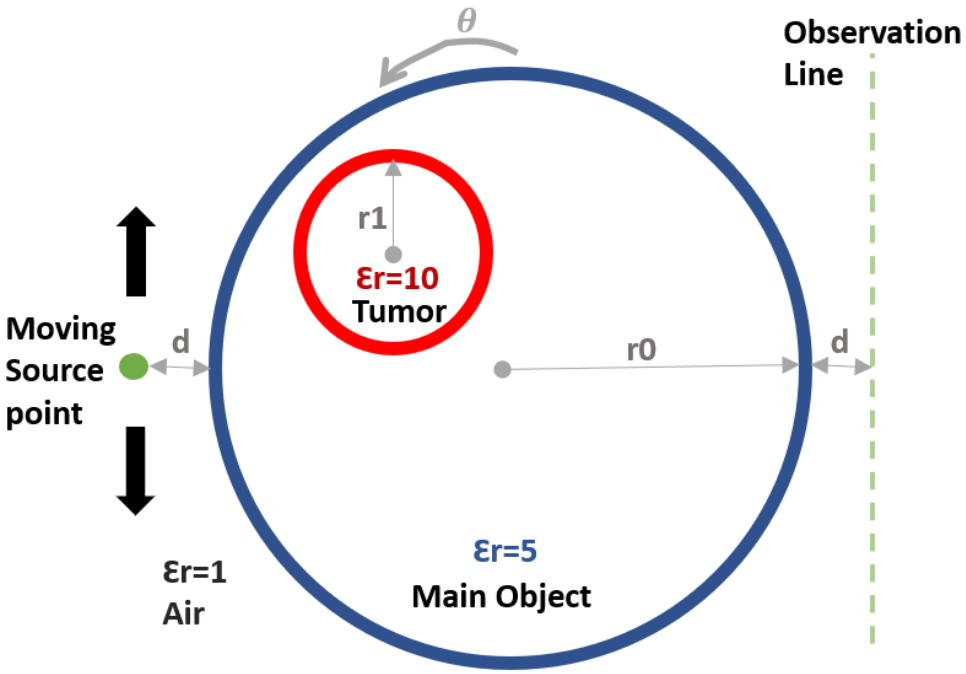

Figure 2.19: The geometry of asymmetric one tumor.

The sinogram profile (Radon) and the reconstructed image are shown in figure (2.20 and 2.21), respectively.

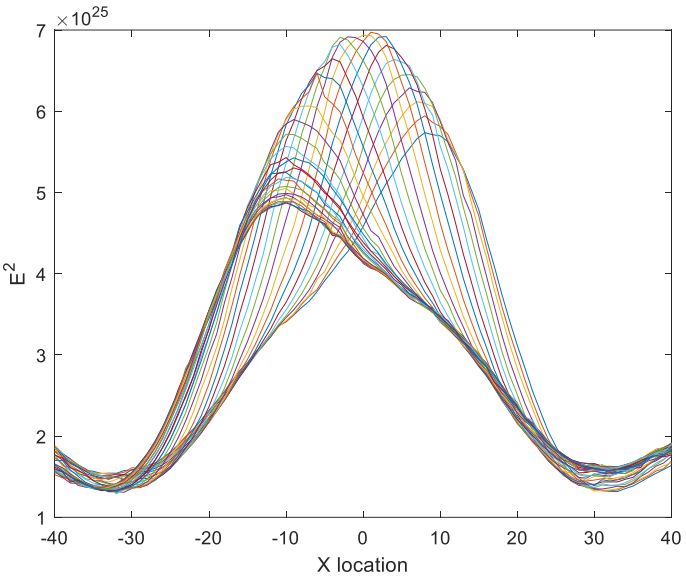

Figure 2.20: The sinogram of the asymmetric case (one tumor).

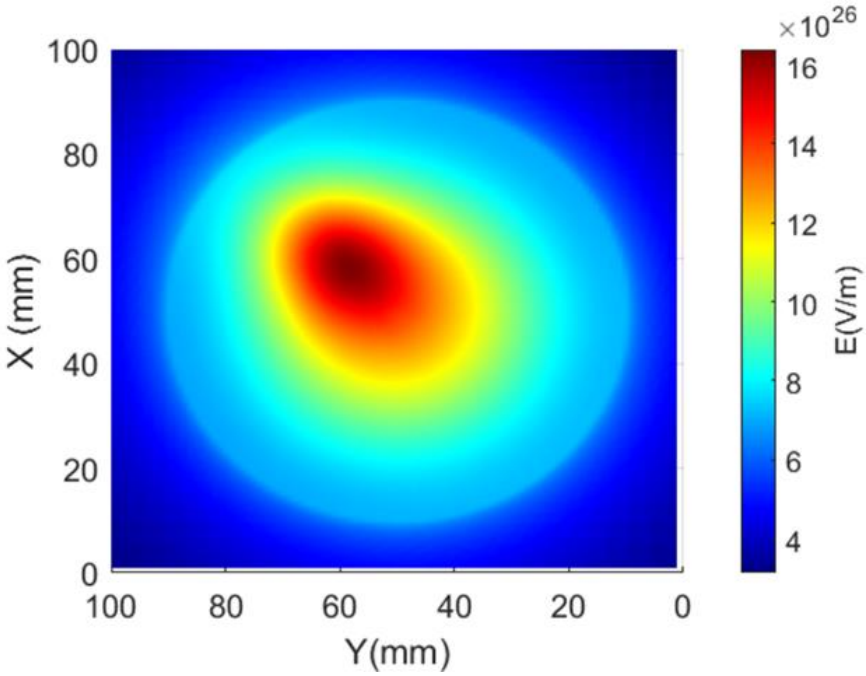

Figure 2.21: The reconstructed image for the asymmetric case (one tumor).

The problem of the elongated image has appeared in this case, as shown in figure (2.21). To solve this problem, the source moving range should start exactly from the position of the radius of the main object plus the distance between the source and the OUT (r0+d). This change in the sweeping range will fix the Axial Ratio (AR=1). Therefore, the reconstructed images after fixing AR problem are shown in figure (2.22).

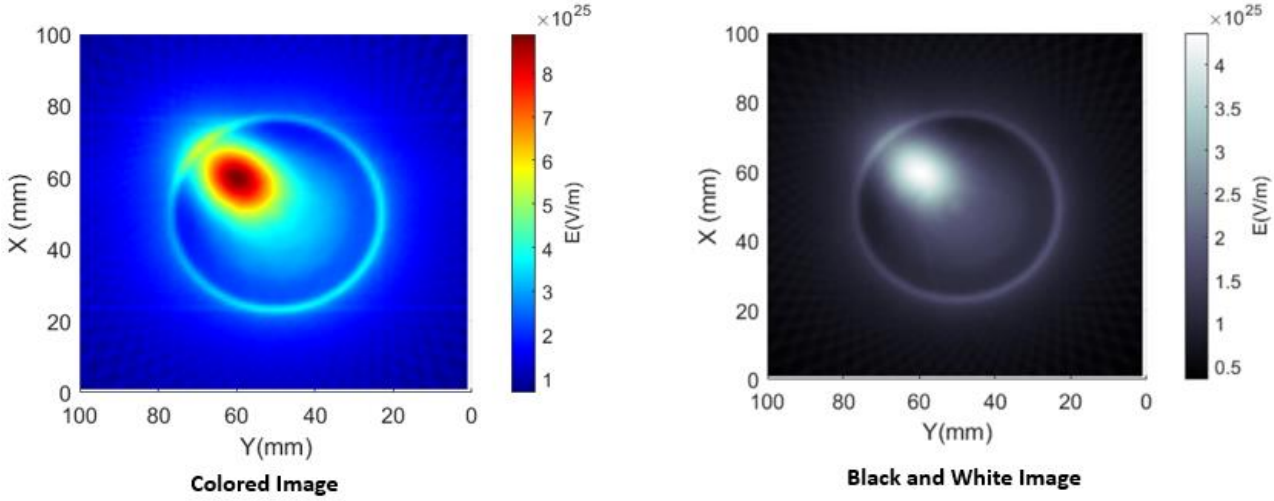

Figure 2.22: The reconstructed image after fixing AR problem.

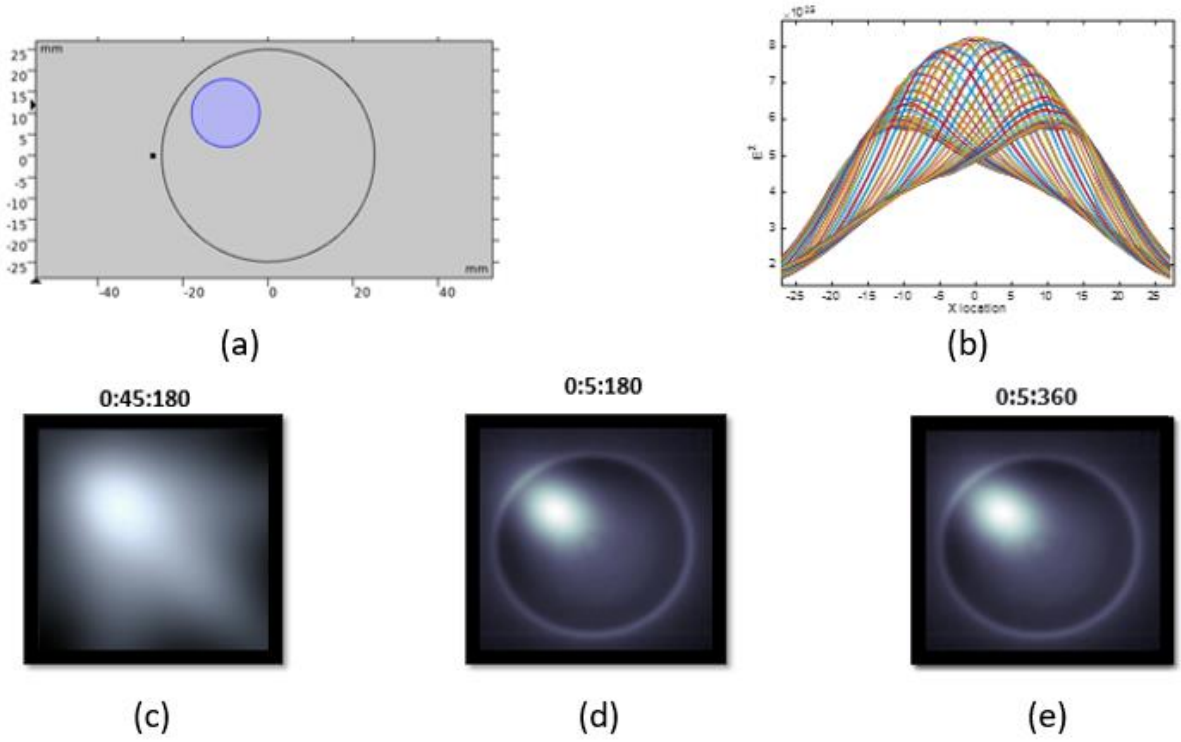

Figure 2.23: Microwave imaging process: a. The original image from COMSOL. b. The Radon transform projections (Sinogram). The reconstructed image: c. from 0 to 180 with an incremental of (45) degree. d. from 0 to 180 with an incremental of 5 degree. e. from 0 to 360 with an incremental of 5 degree.

According to figure (2.23), the resolution of the reconstructed image depends on the incrementalism (rotation step and moving step). In addition, the rotation of (180) degree is not enough to have a clear image because the source that used in this simulation is non-reciprocal source. For this reason, completing the second half (360) is necessary for a sufficient resolution.

2.4.2 Two Asymmetric Tumors

In this case, a second body has been inserted in the main object, as shown in figure (2.24). This new tumor is bigger than the first one, where its radius is equal to (r2=8mm). The other design parameters are similar to table (1).

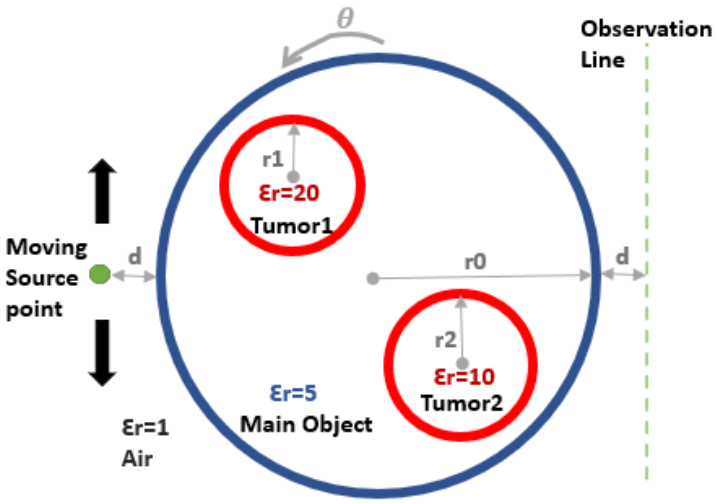

Figure 2.24: The geometry of asymmetric two tumors.

The Sinogram profile (Radon function profiles), and the reconstructed image are shown in figure (2.25 and 2.26), respectively.

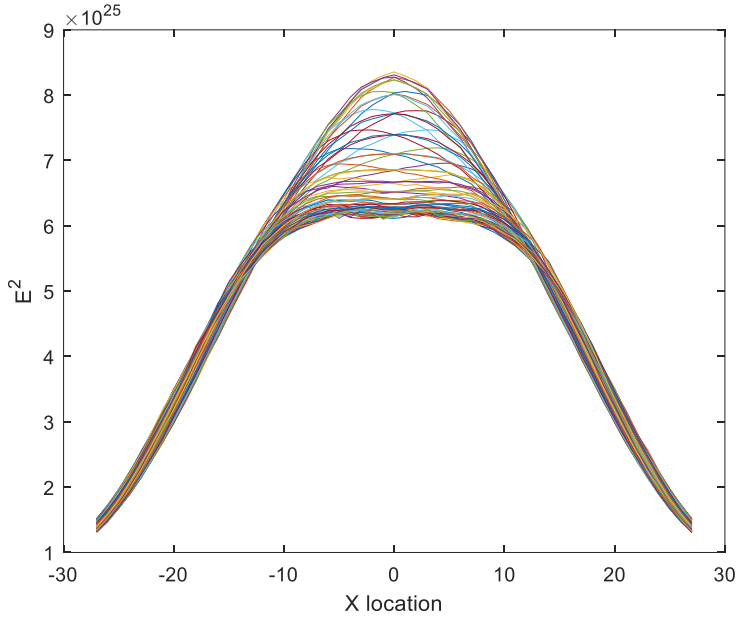

Figure 2.25: The sinogram of the asymmetric two tumors case.

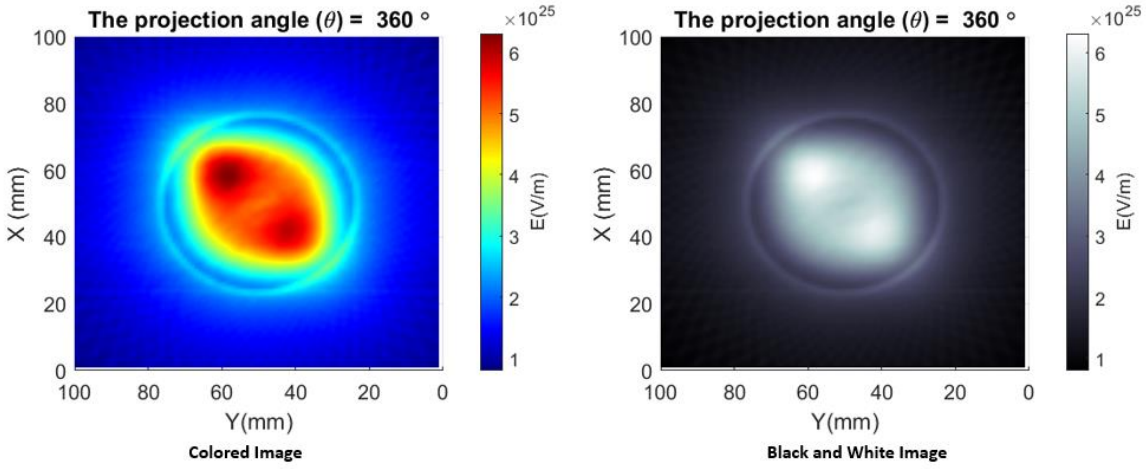

Figure 2.26: The reconstructed images of two tumors case.

As we can see in figure (2.26), Although the size of tumor2 is larger than tumor1, tumor1 has a high intensity in terms of power (dark red color) in the colored reconstructed image because it has the highest relative permittivity.

2.4.3 Three Asymmetric Tumors

In this case, the size of the geometry is increased (the main diameter= 15 cm), and three tumors with different shapes, positions, and permittivity values are inserted into the main body. Figure (2.27) illustrates the case of a large structure and three tumors.

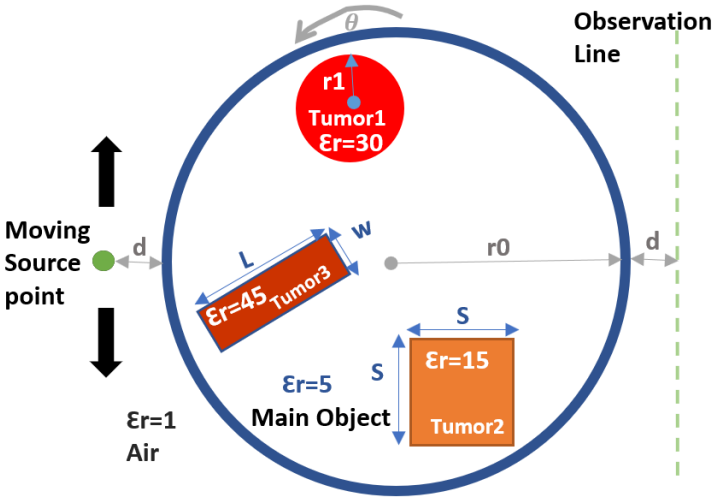

Figure 2.27: The geometry of asymmetric three tumors.

Table (2) shows the design parameters for this case.

Table 2.Three tumors simulation parameters

Parameter	Value
d	2mm
r0	75mm
r1	20mm
L	40mm
w	5mm
θ	0:5:360 deg.
y0	-75:1:75 mm
S	15mm

The Radon function (Sinogram profile) and the rebuilt image are shown in figures (2.28 and 2.29), respectively.

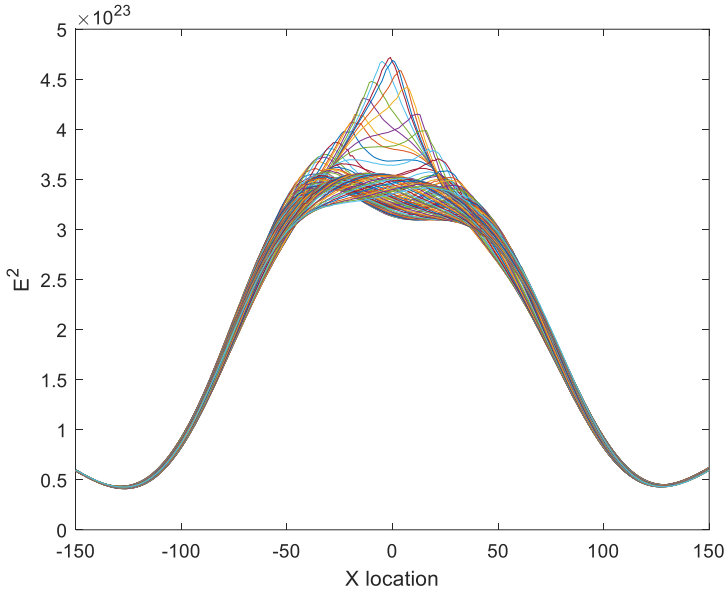

Figure 2.28: The sinogram of the asymmetric three tumors case.

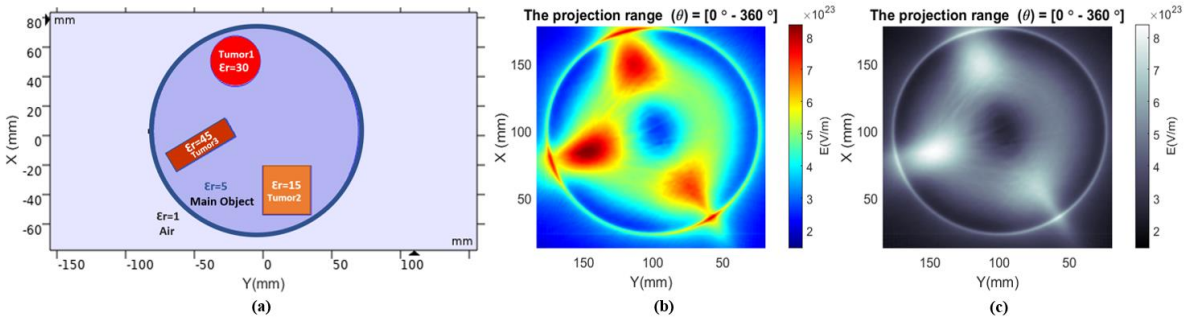

Figure 2.29: The image reconstruction of three tumors case: a. The original image from COMSOL. b. The colored reconstructed image. C. The black and white reconstructed image.

According to the results of this case, we can say that this approach can be used for small or large structures. Where in this work we tried a diameter range (50- 150) mm for the structure, and it gave us a good reconstructed image. Accordingly, an indication of the position of every inserted body and high intensity due to the increase in the relative permittivity value is obvious in the rebuilt images.

2.5 Electrical Conductivity Effect

To test the effect of the electrical conductivity (σ), small spheres made of perfect electric conductor (PEC) are simulated in the air. The electrical conductivity (σ) for each one of the seven circles is equal to (5 S/m), and the radius(r1) is 5mm. Moreover, the radius of the imaginary main circle (r0) is 2.5 cm. Figure (2.30) shows the structure of this simulation.

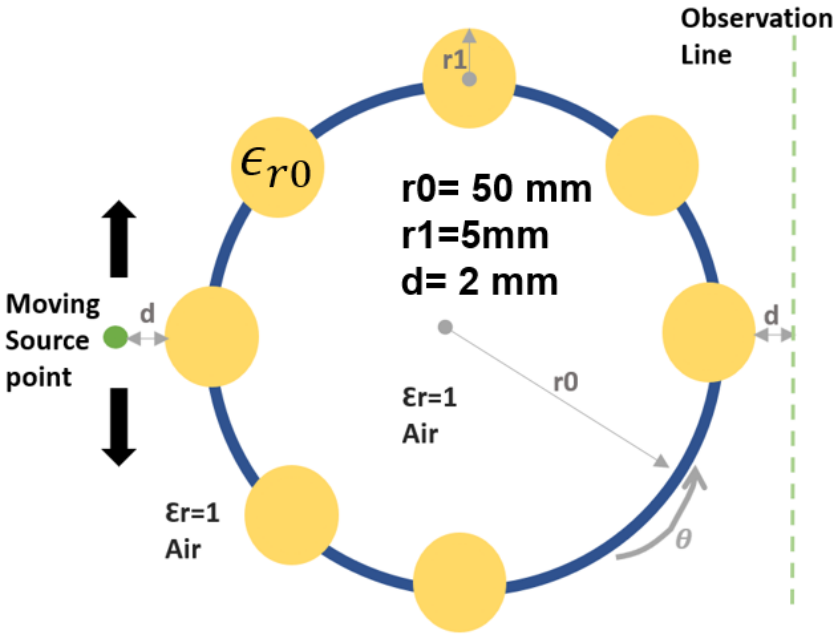

Figure 2.30: The structure of 7-circles in the air.

Furthermore, figure (2.31) shows the results of this case, where the reconstructed image can only detect the permittivity, and the effect of the electrical conductivity (σ) can be ignored in this physic in COMSOL (Electrostatic Physic). The electrical conductivity (σ) will make the reconstructed image blurrier and may affect the resolution. The position of each sphere is shown in the figure (2.29) only when the permittivity of these small circles is higher than the permittivity of the surrounding air.

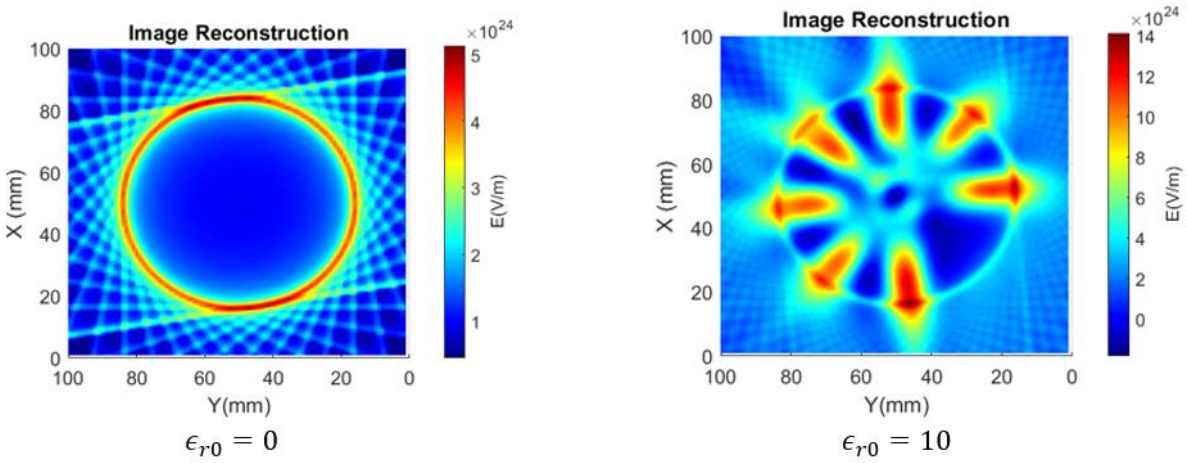

Figure 2.31: The reconstructed image of 7-circles in the air with different circles permittivity values (ε_{r0}=1 & 10) and the same electrical conductivity (σ=5).

Chapter 3
Future Works and Conclusion

3.1 Future Work

This work can be developed by improving the simulation work ((e.g., Full-wave simulation or Magnetostatic simulation) as well as the real experimental Validation especially for asymmetric and in-homogenous cases. Using ESA in the near-field region will help in reconstructing images in reality because of the features of beam-like behavior and high penetration ability[2]. Moreover, to increase the resolution of the rebuilt images, Iterative reconstruction (IR) and Deep learning Iterative Reconstruction (DLIR) techniques will have the potentially to integrate with MI [27]. Likewise, Radon Cumulative Distribution Transform (RCDT)[28] can be applied as an advanced alternative of the Radon Transform (RT)[29]. In addition, further scanning systems such as Fan-Beam and Cone-beam techniques can improve this imaging approach in its short-range scenario[2] and make the reconstruction process faster. Figure (2.30) shows a schematic that demonstrating the operation of the fan-beam scanning system.

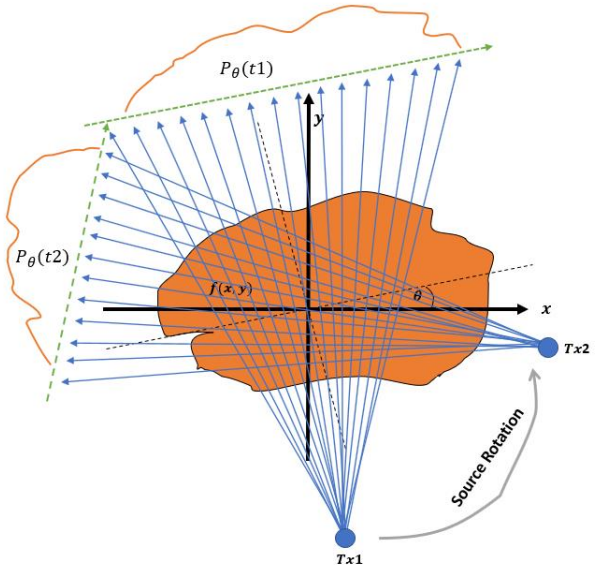

Figure 3.1: Fan-beam scanning technique.

3.2 Conclusion

In this project, a localized source and numerical simulation in Quasi-static environment were developed to model the medical imaging process of human tissue containing either one or more tumors. In this model a movable, localized, and wavelength-independent electrostatic dipole point is used as a ray-like source to detect the inserted tumors. The variation of the electric field (radiated power) of the waves generated from the vertically moving point source that passes through circular-like rotating body around its center is measured.

Thus, the projection profile for each point at an imaginary detection line was registered. Subsequently, Filtered Back Projection (FBP) and Inverse Radon Transform (IRT) algorithms were applied to reconstruct 2-D image of the scanned body. In order to reconstruct the original image, the power profiles at different source movements and different body rotations are added together and processed using inverse Radon transform. Due to the difference in the relative permittivity values of the object and the tumor, different measured power profiles are generated and consequently tumor can be detected. Simulation was performed for inhomogeneous and asymmetric as well as symmetric structures. Results show the ability of the proposed method to successfully reconstruct good resolution image and the capability of distinguishing between tumorous and normal tissues.

The proposed method can be used as an early-stage and inexpensive approach for imaging tumors in human tissues as well as different future applications in different fields.

References

[1] S. S. Ahmed, A. Schiessl, F. Gumbmann, M. Tiebout, S. Methfessel, and L. P. Schmidt, "Advanced microwave imaging," *IEEE Microw Mag*, vol. 13, no. 6, pp. 8–10, 2012, doi: 10.1109/MMM.2012.2205772.

[2] S. H. Mirjahanmardi, "Microwave Near-Field Imaging and Material Characterization.",2020.

[3] C. Pichot, L. Jofre, G. Peronnet, and A.-J.-C. Bolomey, "Active Microwave Imaging of Inhomogeneous Bodies," 1985.

[4] M. A. Aldhaeebi, T. S. Almoneef, A. Ali, Z. Ren, and O. M. Ramahi, "Near Field Breast Tumor Detection Using Ultra-Narrow Band Probe with Machine Learning Techniques," *Sci Rep*, vol. 8, no. 1, Dec. 2018, doi: 10.1038/s41598-018-31046-9.

[5] R. Chandra, H. Zhou, I. Balasingham, and R. M. Narayanan, "On the Opportunities and Challenges in Microwave Medical Sensing and Imaging," *IEEE Transactions on Biomedical Engineering*, vol. 62, no. 7. IEEE Computer Society, pp. 1667–1682, Jul. 01, 2015. doi: 10.1109/TBME.2015.2432137.

[6] C. Pichot, L. Jofre, G. Peronnet, and A.-J.-C. Bolomey, "Active Microwave Imaging of Inhomogeneous Bodies," 1985.

[7] "Society, A. C. Cancer facts and figures 2017 @ONLINE," ,2017.

[8] P. M. Meaney, K. D. Paulsen, and J. T. Chang, "Near-field microwave imaging of biologically-based materials using a monopole transceiver system," *IEEE Trans Microw Theory Tech*, vol. 46, no. 1, pp. 31–45, 1998, doi: 10.1109/22.654920.

[9] S. Shahir, "Near-Field Scattering Tomography System for Object Imaging and Material Characterization."

[10] S. Shahir, B. Semnani, M. Mohajer, G. Rafi, J. Orchard, and S. Safavi-Naeini, "Millimetre-wave multi-view near-field scattering tomography system," *IET Microwaves, Antennas and Propagation*, vol. 12, no. 6, pp. 858–863, May 2018, doi: 10.1049/iet-map.2017.0193.

[11] M. Kim, S. Park, and H.-K. Jung, "An Advanced Numerical Technique for a Low-Frequency Electromagnetic Field Simulation based on the Finite-Difference Time-Domain Method."

[12] S. Shahir, B. Semnani, M. Mohajer, G. Rafi, J. Orchard, and S. Safavi-Naeini, “Millimetre-wave multi-view near-field scattering tomography system,” *IET Microwaves, Antennas and Propagation*, vol. 12, no. 6, pp. 858–863, May 2018, doi: 10.1049/iet-map.2017.0193.

[13] C. Høilund, “The Radon Transform,” 2007.

[14] “Tomographic Image Reconstruction.”

[15] H. Ermert, G. Fulle, and D. Hiller, “Microwave Computerized Tomography,” Nov. 2007, pp. 421–426. doi: 10.1109/euma.1981.333003.

[16] T. M. Grzegorczyk, P. M. Meaney, P. A. Kaufman, R. M. Diflorio-Alexander, and K. D. Paulsen, “Fast 3-D tomographic microwave imaging for breast cancer detection,” *IEEE Trans Med Imaging*, vol. 31, no. 8, pp. 1584–1592, 2012, doi: 10.1109/TMI.2012.2197218.

[17] C. Indd, “The Radon Transform and Medical Imaging 2:43:27 PM.”

[18] C. Indd, “The Radon Transform and Medical Imaging 2:43:27 PM.”

[19] M. B. Biçer, A. Akdaɬli, and C. Özdemir, “Breast cancer detection using inverse radon transform with microwave image technique,” in *2015 23rd Signal Processing and Communications Applications Conference, SIU 2015 - Proceedings*, Jun. 2015, pp. 2182–2185. doi: 10.1109/SIU.2015.7130306.

[20] C. Høilund, “The Radon Transform,” 2007.

[21] J. Larsson, “Electromagnetics from a quasistatic perspective,” *Am J Phys*, vol. 75, no. 3, pp. 230–239, Mar. 2007, doi: 10.1119/1.2397095.

[22] J. Larsson, “Electromagnetics from a quasistatic perspective,” *Am J Phys*, vol. 75, no. 3, pp. 230–239, Mar. 2007, doi: 10.1119/1.2397095.

[23] “User´s Guide Comsol Multiphysics ®.” [Online]. Available: www.comsol.com/support/knowledgebase

[24] “User´s Guide Comsol Multiphysics ®.” [Online]. Available: www.comsol.com/support/knowledgebase

[25] “User´s Guide Comsol Multiphysics ®.” [Online]. Available: www.comsol.com/support/knowledgebase

[26] J. Larsson, “Electromagnetics from a quasistatic perspective,” *Am J Phys*, vol. 75, no. 3, pp. 230–239, Mar. 2007, doi: 10.1119/1.2397095.

[27] F. De, M. E. De, and V. Editors, “Applied and Numerical Harmonic Analysis Harmonic and Applied Analysis From Radon Transforms to Machine Learning.” [Online]. Available: https://link.springer.com/bookseries/4968

[28] J. Lee, R. M. Nishikawa, and G. K. Rohde, “Detecting mammographically occult cancer in women with dense breasts using Radon Cumulative Distribution Transform: a preliminary analysis,” Feb. 2018, p. 7. doi: 10.1117/12.2293541.

[29] W. C. Chew and Y. M. Wang, “Reconstruction of Two-Dimensional Permittivity Distribution Using the Distorted Born Iterative Method,” *IEEE Trans Med Imaging*, vol. 9, no. 2, pp. 218–225, 1990, doi: 10.1109/42.56334.

[30] MATLAB. Matlab Program@ONLINE, September 2020.

Appendices

Appendix A

MATLAB Code for Asymmetric Cases

```
%%%%%%%%%%%%%%%%%%%%%%%%%%%%%%%%%%%%%%%%%%%%%%%%%%%%
% This code is for Medical Imaging Using Electrostatic Dipole point %
% and Inverse radon Transform.                                      %
%%%%%%%%%%%%%%%%%%%%%%%%%%%%%%%%%%%%%%%%%%%%%%%%%%%%
clear all;
clc;
format long

%%% ###Input Parameters###:
% Number of steps from Comsol
n_steps = 71;
% step value
x_step=1;
% Number of accuracy value from simulation data
n_accuracy = 71;
% X-Axis Limit value
xl=35;
% Number of files
nf=19;
% Degree step value
deg=10;

% Creating a video
obj=VideoWriter('Imaging.avi');
obj.Quality=100;
obj.FrameRate=20;
open(obj);

% Calculating the periodicity
perd =(n_accuracy - 1)/ (n_steps - 1);

% The sweeping range
x1 = (-xl:x_step:xl);

% Importing Data files
mydata = cell(1, nf);
for k = 1:nf
  myfilename = sprintf('data (%d).txt', k);
  mydata{k} = importdata(myfilename);
  E{1,k}=mydata{1,k}  ;

end

%Making a matrix for all angles
```

```
for j=1:x_step:(n_accuracy)

    for k=1:nf

          B1(j,k) =E{1,k}(1*(j-1)+1,j+1);
    end
end

%###ploting X_Locatin Vs. E^2

figure (1)
plot(x1,B1)
xlabel('X_Locatin');
ylabel('E^2');
%%## Making on Table ( X_Locatin Vs. E for each angle)
A3 = [x1.', B1];

%% ## Appling Inverse Radon
A4 = zeros(100,100);
output_size = max(size(A4));
% tic
for i=1:nf
   A4 = A4 + iradon([x1.', B1(:,i)],(i-1)*deg,'Ram-Lak',output_size);
% filters: None , hamming , hann , Ram-Lak
%%## Ploting the Image and recording the animation
figure (2)
% surf(1-A4)
surf(A4)
view(-90,90)
colormap Jet
% bone , Jet , gray , copper
shading interp
xlim([0 100])
ylim([0 100])
 c = colorbar;
c.Label.String = 'E(V/m)';
xlabel('X (mm)')
ylabel('Y(mm)')
set(gca,'FontSize',10)
% title('Image Reconstruction');
title(['The projection angle (\theta) =  ',num2str(deg*(i-1)),' \circ']);
fig2=figure (2);
F=getframe(gcf);
writeVideo(obj,F);
end

%%Ending the recording
obj.close();

%%%%%%%%%%%%%%%%%%%%%%%%%%%%%%%%%%%%%%%%%%%%%%%%%%%%%%%%%%%%%%%%%%%%%%%%%%%%%%%
```

Appendix B

MATLAB Code for Symmetric Cases

```
clear all;
clc;
format long
n_steps = 71;
x_step=1;
n_accuracy = 71;
perd =(n_accuracy - 1)/ (n_steps - 1);
% X-Axis Limit
xl=35;
% Number of files
A = dlmread('Centre71point.txt');
E = A;
x = E(:,1);

for i=1:x_step:(n_accuracy)
B1(i) = E(perd*(i-1)+1,i+1);
end

x1 = (-xl:x_step:xl);
plot(x1,B1)
xlabel('X location');
ylabel('E^2');
A2 = [x1.', B1.'];
A4 = zeros(100,100);
output_size = max(size(A4));
for i=1:360
   A4 = A4 + (iradon(A2,(i),'hamming',output_size));
% filters: None , hamming , hann
end

figure
surf(A4)
view(-90,90)
colormap(turbo)
xlim([0 50])
ylim([0 50])
% colormap bone
shading interp
xlim([0 50])
ylim([0 50])
 c = colorbar;
c.Label.String = 'E(V/m)';
xlabel('X (mm)')
ylabel('Y(mm)')
set(gca,'FontSize',15)
```